Synthesis of hybrid microgels for the degradation of 4-Nitrophenol and dyes

A dissertation submitted to the Department of Chemistry,
Quaid-i-Azam University, Islamabad, in partial fulfillment
of the requirements for the degree of

Master of Philosophy

in

Physical Chemistry

by

Abdul Haleem

Department of Chemistry
Quaid-i-Azam University
Islamabad
2015

IN THE NAME OF ALLAH

THE COMPASSIONATE

THE MERCIFUL

Dedicated to

My Respected and Loving Parents

TABLE OF CONTENTS

ACKNOWLEDGEMENTS

All praises to almighty **ALLAH** the benevolent, who bestowed upon me. His blessings and through the mediation of his beloved **Prophet Muhammad** (**peace be upon him**) enlightened me with abundant resoluteness and perseverance, that enabled me to accomplish this scientific assignment objectively and successfully.

I am not able to find appropriate words to offer my humble thanks and pay my immense gratitude to my most respected and worthy **supervisor** and **chairman of chemistry department Professor Dr. Mohammad Siddiq**, who showed commendable alacrity in providing proper guidance and encouragement. His support through educative discussion and scientific suggestions made this research work to be an extremely purposeful venture for me personally.

I am also thankful to **associate Professor Dr. Hazrat Hussain, head of physical section**, for providing me all necessary facilities during the completion of this research work.

I am grateful to my friends and lab-fellows, **Dr. Luqman Ali Shah, Mohib Ullah, Usman Saeed, Shaheed Ullah** and **Hasseb Ullah** for their kind cooperation and assistance during my research wor*k.*

Here I cannot forget my family i.e. **my parents, my brothers, sisters** and specially my elder brother **Khalid Rehman** and cousin **Muhammad Rehman**. My parents always helped me and encouraged me against all odds and gave me the confidence to stand where I am today.

I am thankful to all the well wishers who helped me in areas where I got stuck up during this research undertaking.

Abdul Haleem

ABSTRACT

Ter-copolymer microgel poly(N-isopropyl acrylamide-*co*-methacrylic acid-*co*-2-hydroxyethyl methacrylate) was synthesized by free radical emulsion polymerization and purified by dialysis. The silver and gold nanoparticles were prepared by insitu chemical reduction using sodium borohydride as reducing agent at 10 and 40 °C. FT-IR spectroscopy confirms the microgel synthesis and existing of silver and gold nanoparticles inside the polymer network. Dynamic Light Scattering was used to determine the size of the microgel particles at different temperatures and pH. Scanning Electron Microscopy (SEM) was carried out for the determination of particle size and morphology. X-Ray Diffraction (XRD) was used to investigate the synthesis of pure and hybrid microgels. The hybrid microgels were successfully applied as a catalyst for the reduction of 4-nitrophenol and for the degradation of organic dyes i.e. Congo red, Methylene blue and Eosin Y. The effect of temperature on the apparent rate constant is also the part of this work.

LIST OF TABLES

LIST OF FIGURES

Chapter-1
Introduction

Polymer properties are generally divided into several classes based on the scale at which the property is defined as well as upon its physical basis [1].The most important property of a polymer is the individuality of its basic monomers. A second set of properties, essentially explain the arrangement of these monomers within the polymer at the scale of a single chain. These basic structural properties play a key role in determining bulk physical properties of the polymer, which explain how the polymer behaves as a continuous macroscopic material. Chemical properties, at the nano-scale, illustrate how the chains interact through various physical forces. At the macro-scale, they express how the bulk polymer interacts with other chemicals and solvents.

1.1 Polymer Gels

The colloidal solutions composed of distribution of liquid part within a solid component such that the solid component act as a continuous phase and the liquid as the discontinuous phase are called gels [2]. Polymer gels are formed by the combination of polymer chains in a three dimensional structure in which the solvent molecules are present inside the network. By weight, gels are mostly liquid, yet they behave like solids due to a three-dimensional cross-linked network.

1.1.1 Classification of Polymer Gels

Polymer gels can be classified in many ways but based on their size there are two types of polymer gels.

(i) Macrogels

Macrogels have the large molecular weight and size is from 1000μm up to few millimeters [3, 4]. Because the size is very large due to which very slight reversible change is observed in their structure. When the monomers composition is very high then macrogels are formed. Macrogels are also called bulk molecules or macro molecules.

(ii) Microgels

Microgels or nanogels are cross linked particles that have particle size in nano range (20-1000 nm). Due to their small size they have large surface area, high water

content, tunable size, due to these properties they are used for many applications especially in nanoreactors and biomedical fields [5, 6].

Microgel was first prepared by Staudinger Husemann but the term microgel was used for the first time by Barker so this is the new field for researcher in 1995 [7]. Microgels are stimuli-responsive cross linked polymeric network materials which allow the integration of stimuli- responsive properties into the gel. Due to these properties they are classified into two categories (a) physical stimuli such as temperature, light, magnetic or electric fields and (b) chemical stimuli such as ionic strength, pH, or the presence of biological or chemical compounds. The microgels change their properties if we change the above conditions. Due to these properties the microgels are also called "smart" materials.

Due to the responsive behavior these materials has led to a tremendous applications including sensors [8], optics [9], colloidal crystals [10, 11], cell culture substrates [12] and for drug delivery [13].

1.1.2 Classification of Microgels

On the basis of various parameters e.g. composition, sensitivity and chemical nature microgels can be classified into the following groups.

(1) Classification based on Cross linkers

On the basis of cross linker microgels are of two types.

(a) Physical Cross Linked Microgels

In this cross linking the physical forces play vital rules and bind the polymer chains closed to each other [14]. The physical forces may be vander Waal forces, hydrogen bonding and may be any other interactions which play a vital rule in pH and temperature change by changing external stimuli [15]. A general sketch for physical microgel is given in **Figure 1.1.**

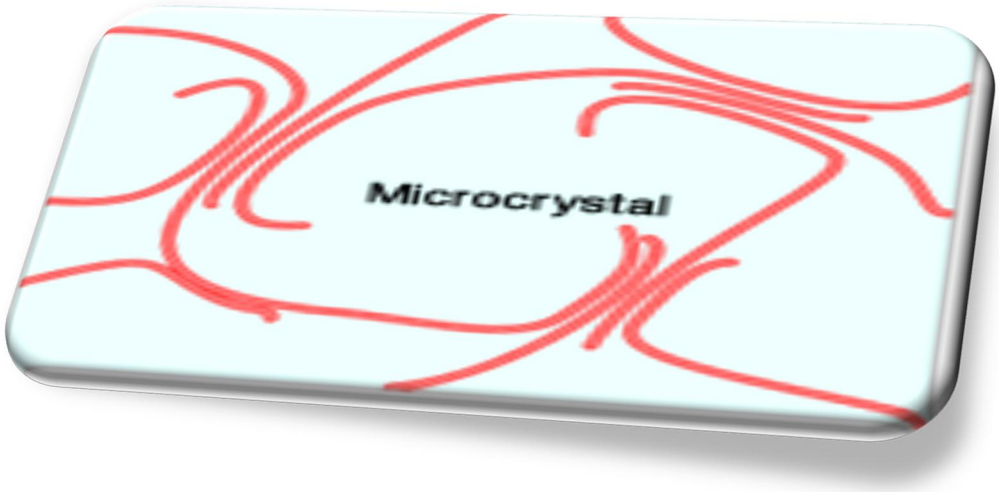

Figure 1.1.Physical cross linking

(b) Chemical Cross Linked Microgels

In chemical cross-linked microgels a multifunctional chemical material used which hold the polymer chains by chemical bonds, mostly covalent bonds [16]. In some cases monomers act as self-cross linker [17] also, a general sketch is given in **Figure 1.2.**

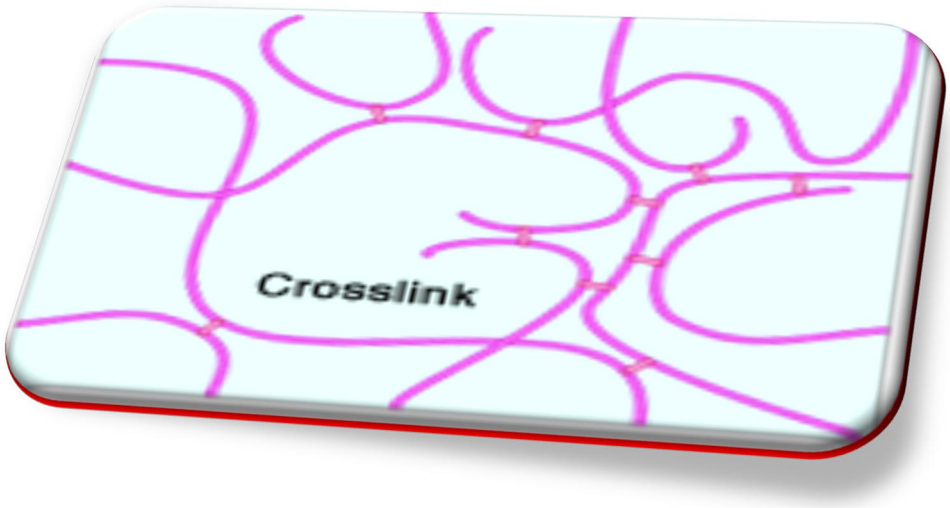

Figure 1.2. Chemical cross linking

(2) Classification based on Composition

On the basis of composition, the microgels are of three types.

(a) Homopolymeric Microgels

The microgels formed by polymer chains composed of only one type of monomers are called Homopolymeric microgels e.g. poly (N-isopropyl acrylamide) in which all the monomers are NIPAM.

(b) Heteropolymeric Microgels

The microgels in which two or more than two different type of monomers are present in polymer chains involved in network formation are called Heteropolymeric microgels e.g. the microgel of (2-Hydroxyethyle methacrylate) HEMA and NIPAM is called Heteropolymeric microgel because in this microgel two different monomers combine with each other.

(3) Classification of Microgels on the basis of response

On the basis of responsive behavior microgels can be divided into the following groups.

(a) Non-responsive Microgels

The microgels which have the ability to retain their integrity upon the exposure to various stimuli are called non-responsive microgels.

(b) Stimuli-responsive Microgels

The microgels which undergo properties change by the application of external stimuli are called stimuli-responsive microgels. Based on the type of stimulus applied, these microgels are further classified in many types i.e. temperature, pH, ionic strength, concentration of salts, electric and magnetic fields, reduction and oxidation responsive microgels etc [18, 19]. These effects are summarized in **Figure 1.3**.

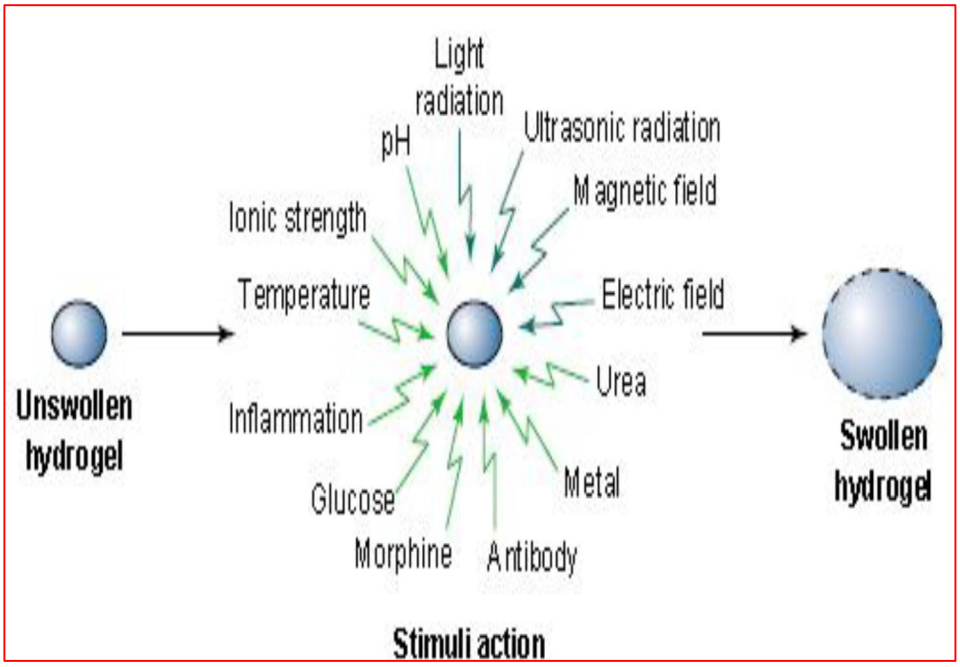

Figure 1.3. Effect of different external stimuli on size of microgel

Our work is concerned with temperature and pH sensitive, therefore we are going to explain the properties change by changing these stimuli.

(i) Thermal-responsive Microgels

The microgels which show response to temperature are called temperature responsive or thermal responsive microgels. Due to change in temperature they show change in their size and structure. The microgels which increase their size with the enhancement of temperature are called positive temperature responsive microgels, while if the size decreases with increase of temperature than these microgels are called negative temperature responsive microgels. In 1986 Pelton and Chibante [20] first time reported N-isopropyl acrylamide (NIPAM) as a negative thermo responsive monomer. The lower critical solution temperature (LCST) of NIPAM is 32^{o}C [21, 22, 23]. Above the LCST the NIPAM is hydrophobic due to isopropyl group [24, 25] and shows hydrophilic property below the LCST due to the presence of amide group. The chemical structure of NIPAM is given below,

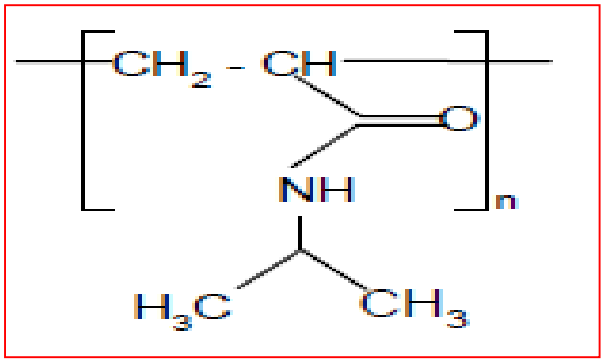

Above the LCST the microgel is in collapse state because at high temperature the water molecules expel to the exterior because the interaction between water molecules and polymer chains become weak, and the interaction between polymer-polymer chains become dominant. But at low temperature the interaction between the water molecules and the polymer chains become dominant over the polymer-polymer chain interaction, which causes the water molecules penetrate inside the network and increase in size [26,27].

(ii) pH-responsive Microgels

The microgels which are sensitive towards pH change are called pH responsive microgels [28]. pH responsive microgels are of two types (a) anionic microgels(b) cationic microgels.

(a) Anionic Microgels

Anionic microgels formed with acidic functional groups containing monomers and shows responsive behavior towards pH change e.g. P(AA), P(MAA) etc are highly responsive to the pH change because in these microgels there are present acid functionalities such as carboxylic group. The pKa value of the monomer acts as a bridge for the conversion of polymers from one state to another with pH change. AA and MAA exist in protonated form at low pH, and deprotonated form at high pH. When we increase the pH proton is released and negative charge creates on polymer network which repel each other and size increase, the decrease in pH causes reduction in particle size. A general representation for pH change is given in **Figure 1.4.**

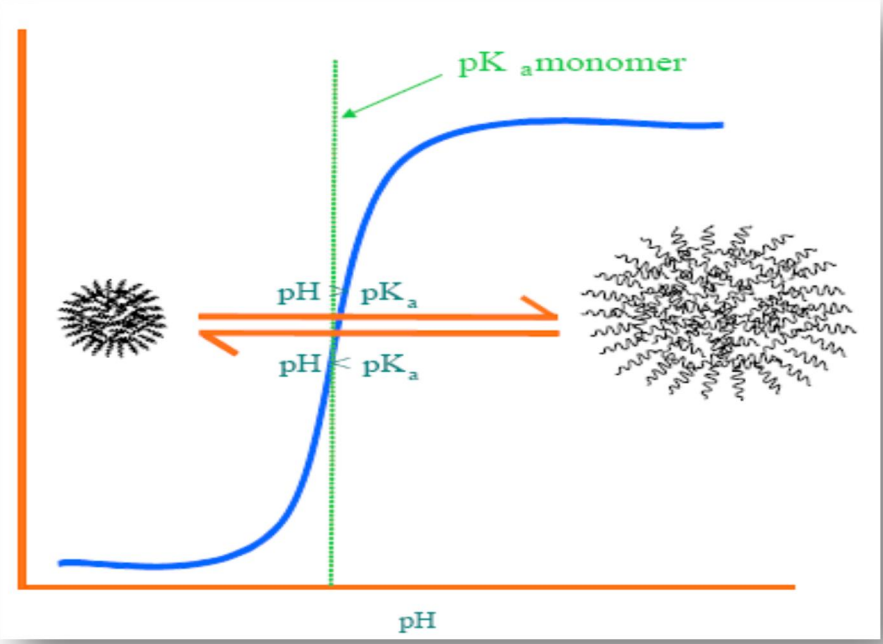

Figure 1.4. Cartoon showing transition associated with pH responsive microgel

(b) Cationic Microgels

The microgels formed by monomers composed of basic functional groups are called cationic microgels e.g. poly(2-vinylpyridine), poly(vinylamine), poly(vinylimidazole), poly(2-diethylaminoethyl methacrylate) P(DEAEMA) and poly(N, N-dimethylaminoethyl methacrylate) P(DMAEMA) [28].

1.2 Hybrid Microgels

Materials formed by the combination of pure microgels with inorganic nanoparticles are called hybrid microgels. The particles may be silver, gold, copper, cobalt, nickel etc. They hybrid materials playing a key role in a lot of applications e.g. drugs delivery, optics and especially used in catalysis [29].

1.2.1 Application of Hybrid Microgels

(A) Microgels as a Microreactor

One of the most significant properties of noble metal nanoparticles is their catalytic activity for some organic reactions due to their small size [30]. But due to the problem of their easy aggregation, the recycling of the nanoparticles is difficult. To

overcome this problem there should be some suitable carrier systems [31] otherwise, the product would be greatly affected by residual metal nanoparticles, and increase its expenditure. We used polymer microgels as reactor for the formation of metal nanoparticles and then carried out some reactions using these hybrid materials as a catalyst. A general representation is given in **Figure 1.5.**

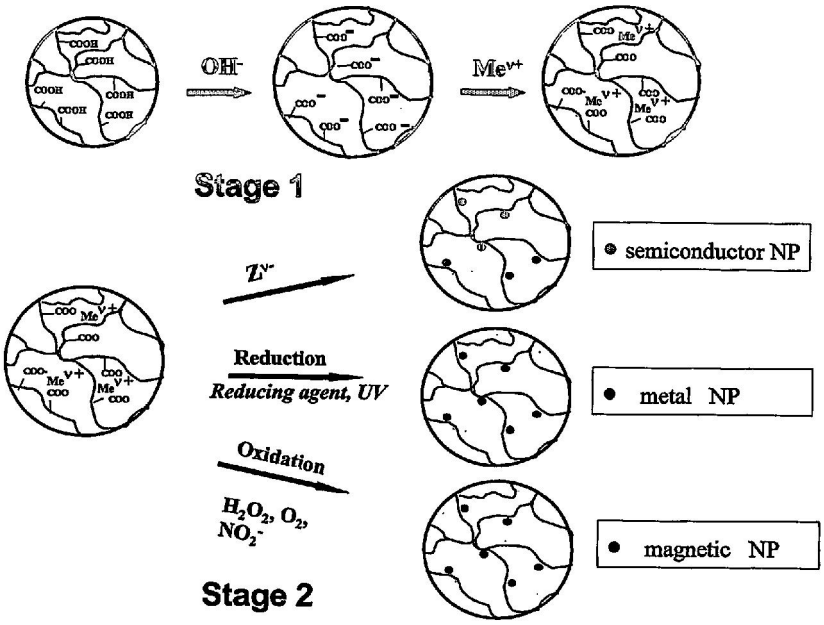

Figure 1.5 Formation of hybrid microgels by different routes

(B) Microgel used in Drug Delivery

Drug delivery system (DDS) is very necessary for drug transport and release. The drug is loaded on the nanoparticles in the microgel through covalent interaction or non covalent interaction. Gold nano particles (AuNPs) are an excellent carrier system for DDS design due to the functional adaptability of their monolayer which is shown in the sketch below. The Au NPs can be delivered to the targeted site using hybrid microgels.

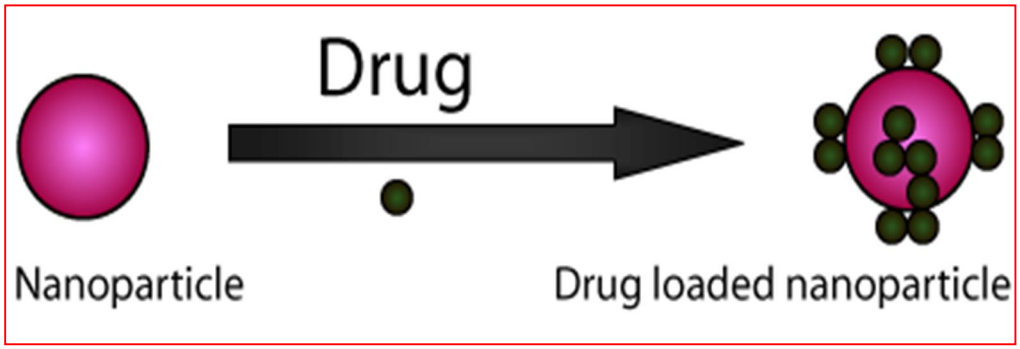

1.3 Literature Survey

For instance, Lu et al. [32] reported a core–shell structured carrier based on polystyrene (PS) as core and Ag nanoparticles loading poly(Nisopropylacrylamide) (PNIPAM) network as shell, in which the catalytic activity of the Ag nanoparticles can be modulated by temperature. However, preparing the carrier is difficult and the content of Ag nanoparticles within its shell is limited. Lin et al. [33] utilized hollow PNIPAM microgel as the carrier of Ag nanoparticles for controlling their catalytic activity by temperature. Similarly, it is hard to prepare the carrier with hollow structure. Moreover, the Ag nanoparticles entrapped within its cavity are easy to aggregate. Dong et al. [34] successfully fabricated poly(N-isopropylacrylamide-co-acrylic acid) (poly(NIPAAm-co-AAc))-stabilized Ag NPs within microgel particles using $NaBH_4$ as a reducing agent. Mohn et al. [35] reported the fabrication of Ag NPs in semi-interpenetrating network hydrogels made of poly(NIPAAm-co-NaAcrylate). Coradin and coworkers [36] reported the bio-inspired formation of multi-scaleporous silica materials using arginine-based biosurfactants as structure templating and silica polymerization activation. Corma et al. [37] demonstrated the biomimetic synthesis of microporous and mesoporous silica materials by using a mimic of silicatein for silica deposition. Recently, Puchol et al. [38] reported that mesoporous silica nanoparticles of around 100nm diameters could be formed by using solid flakes of chitosan as additive and surfactants as structural directing agents.

Aslan et al. developed a wavelength-ratiometric resonance light scattering technique for glucose sensing based on AuNPs aggregation and dissociation. Instead of absorption signals, the plasmon resonance scattering signals of AuNPs are analyzed for glucose sensing [39].

Shibayama et al. [40] studied the pH and salt concentration of poly(NIPAAm-*co*-AAc) microgels in microscopic structure by using small-angle neutron scattering (SANS) technique and discriminated between the effects of salt and pH on the gel structure and swelling behavior.

Mishra et al. [41] reported the synthesis of Ag nanomaterials with elongated structures in a two phase system using hexadecylamine, whereas Chen et al. [42]

obtained monodispersed silver nanoparticles (12 nm) on a large scale in a simple oleylamine–liquid paraffin system.

Liu et al. [43] used polystyrene particles functionalized by sulfonic and carboxylic groups for modification with PPy and no colloidal destabilization was observed. Recently, Luqman et.al synthesize dual responsive P(NIPA-co-VI)s-Ag hybrid microgels and used the hybrid materials at the entire pH range for the catalytic reduction of p-nitrophenol to p-aminophenol. The catalysts were more efficient at pH 2.95 at high temperature but show reduced catalytic activity at pH 9.32 with high temperature [44].

In the present work we used ter-copolymer P(NIPAM-MAA-HEMA)microgel as a stabilizer for the synthesis of Ag and AuNPs at different temperatures. Their catalytic activity was studied for the reduction of 4-nitrophenol to 4-aminophenol and for the degradation of organic dyes i.e. congo red (CR), methylene blue (MB) and eosin Y (EY) by $NaBH_4$. The temperature effect on catalytic activity is also studied. The hybrid microgels of silver and gold are thermally and chemically stable and show good catalytic activity.

Chapter-2
Characterization techniques

Spectroscopic Techniques

Spectroscopy is a general term in which electromagnetic radiation interacts with matter**.** How these radiations interact with matter is directly depend on the energy of radiations. Ultraviolet and visible wavelengths of higher energy greatly affect the outer electrons in outer shells. Infra red radiation is absorbed by matter causing rotation and vibration in molecule. Radio waves are very weak electromagnetic radiations and only cause spin of nuclei in the presence of magnetic field. As the wavelength decreases the energy of the radiation increases as shown in the following **Figure 2.1**.

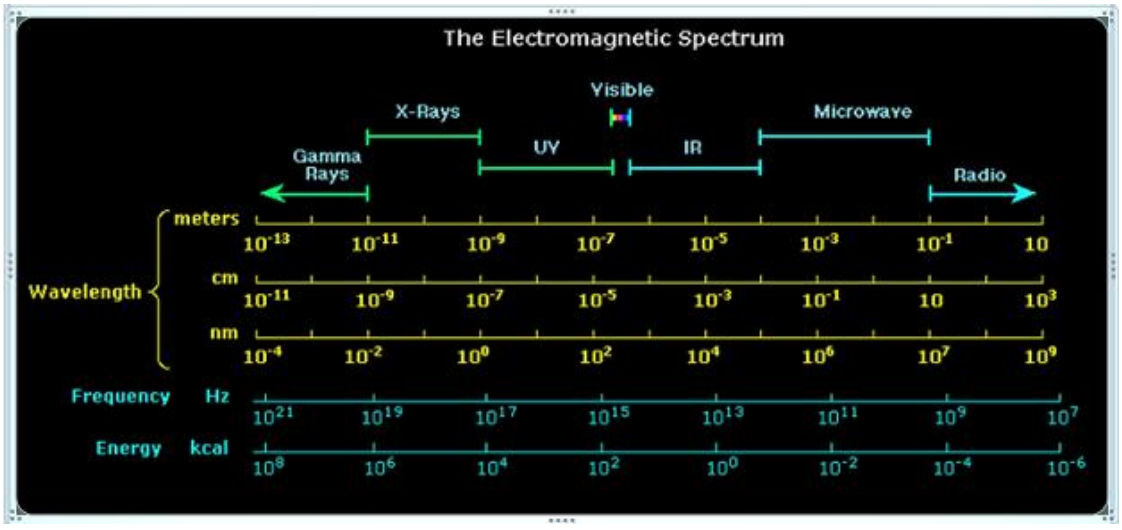

Figure 2.1.Electromagnetic spectrum

2.1 Fourier Transform Infra Red (FTIR) Spectroscopy

This technique provides information about the structure in terms of functional groups of the prepared materials, may be organic or inorganic in nature. In this technique infrared radiation passed through the sample which absorbed some of the radiation and transmit the remaining radiations, gives the results in the form of spectrum. There are two region of IR spectroscopy, frequency region and finger print region. Advantage of this technique is that no two molecules have the same finger print spectra. This technique is used for the analysis of several types of molecules [45].

FTIR spectroscopy is based on the attribute frequencies linked with every bond. Different wavelength of radiations emitted from the source, passes through the modulator and the sample. Sample gives information through the detector. A simple sketch indicating the basic operational components of FTIR spectrophotometer is given below [46].

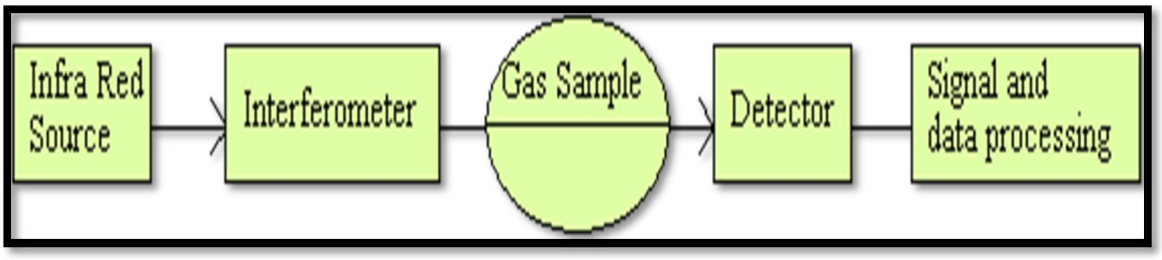

2.2 UV-Visible Spectroscopy

The UV radiation falls in the range of 10 to 400nm while the visible region covers from 400 to 800nm on the electromagnetic spectrum. From 200nm to 400nm range is called near UV region and below 200nm range is called far UV region and is studied under vaccum condition. The possible trasitions takes place in UV-Visible spectroscopy are shown in **Figure 2.2.**

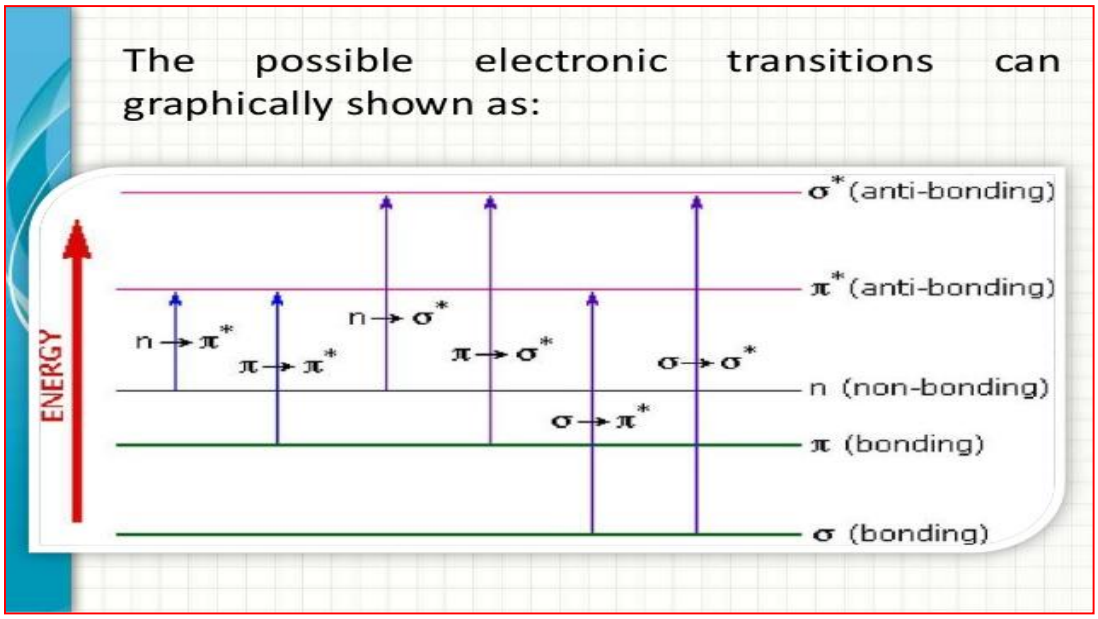

Figure 2.2. Various possible transition

2.2.1 Important Terms used in UV-Visible Spectroscopy

(i) Chromophore

The functional group which is responsible for giving color to the compound or that part of the molecule which absorb radiations above 200nm due to n to π^* and π to π^* e.g. NO_2, N═O, C═O, C≡N, C≡N etc.

(ii) Auxochrome

The other group which attaches with chromophores and affect their light absorbing capacity is called Auxochrome or other functional group which attaches with non bonding electrons and does not absorb the radiation near UV region but when attach with chromophores alter the wavelength of absorb radiation e.g. benzene absorb radiations in 255nm but when OH is attached with benzene ring then they absorb radiations in 270nm. In this example OH act as Auxochrome.

(iii) Bathochromic Shift (Red Shift)

When λ_{max} go toward longer wavelength this is called Bathochromic shift or red shift. This is due to presence of Auxochrome or by changing the solvent e.g. groups like –OH, $-OCH_3$ absorbs radiation in longer wavelength.

(iv) Hypsochromic Shift (Blue Shift)

When λ_{max} go toward shorter wavelength then this is called Hypsochromic sift or blue shift and this is due to the presence of such group which remove the conjugation or by changing the solvent e.g. Aniline show blue shift in the presence of acidic medium due to removal of double bond from Aniline and the wavelength shift from 280nm to 265nm.

(v) Hyperchromic Effect

When absorption intensity increases then this is called Hyperchromic effect. When there is present Auxochrome in the molecule then this effect occur e.g. pyridine absorb radiation in the range of 257nm but 2-methyl pyridine absorb radiation in the range of 260nm due to the presence of Auxochrome ($-CH_3$).

(vi) Hypochromic Effect

When absorption intensity decreases then this is called Hyperchromic effect. When there is present Auxochrome in the molecule then this effect occur e.g. naphthalene absorption intensity is 19000 but the absorption intensity of 2-methyl naphthalene is 10250 due to the presence of Auxochrome ($-CH_3$).

The above four effects are shown in the following **Figure 2.3.**

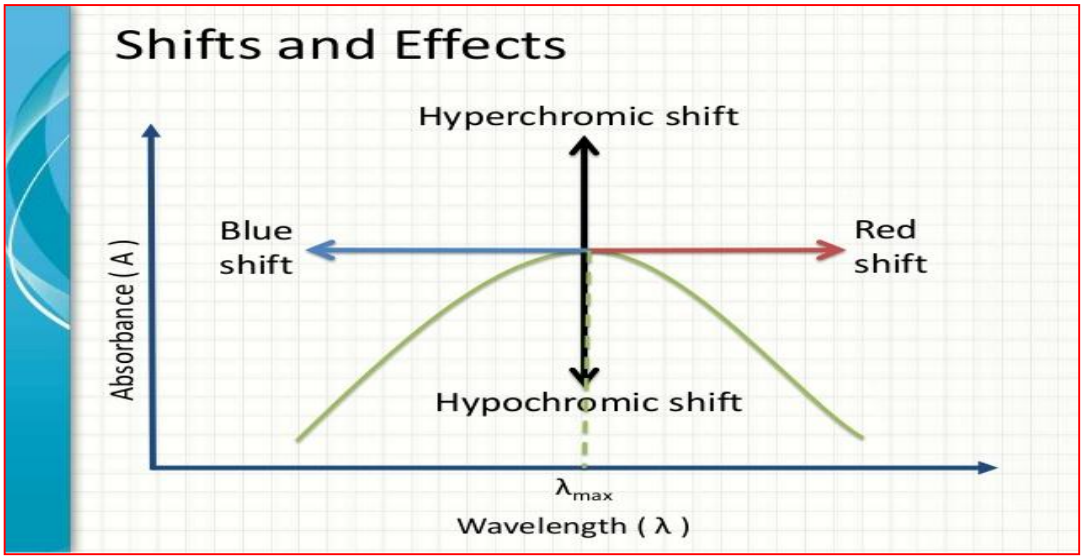

Figure 2.3.Various term used in UV-visible spectroscopy

2.2.2 Instrumentation

The important parts of spectrophotometer are source of light, Monochromator and detector.

There are two types of spectrophotometers; single beam and double beam.

In single beam only one beam is passing through the sample selected for characterization.

In double beam spectrometers the light reaching the sample is divided into two beams. One is passing through that cell in which solvent is present and used as reference, while the other beam passed through the cell in which the solution is present.

2.2.3 Applications of UV-Visible Spectroscopy

UV-Visible spectroscopy is used for both qualitative and quantitative analysis e.g. characterizing aromatic compounds, conjugated olefins, molar concentration of the solution and the formation of metal nanoparticles etc [47].

2.3 Dynamic Laser Light Scattering (DLLS)

Dynamic light scattering is a technique which can used to determine the size and distribution profiles of polymers and polymer gels in solution or small particles in suspension [48].

2.3.1 Light Scattering

In light scattering, a change in the intensity as well as direction of the scattered light takes place after striking particle in its way. This is the basic working principle of the laser light scattering instrument (LLS). Theories which are used to demonstrate this process like Rayleigh scattering, Mie scattering etc. In general scattering is due to a particle, when electrons particle absorb light energy after striking it, and then re-emit without any change. The molecules in the solution exposed to light are being hit and they diffract the light in all directions. Here energy remains constant and there is only change in direction of propagation of light and intensity. This is due to refraction, adsorption, effect of diffraction and reflection of light. When radiations are absorbed by scattering non-involved molecule, in this case law of conservation of energy will not obey.

2.3.2 Laser Light Scattering

The type of source of light used in light scattering is a powerful and coherent beam of laser; thus the term laser light scattering is applied. The progress of the light scattering into laser light scattering has developed this field so an extent that scientists are now using spectrum analyzers and auto-correlators to study the motions and frequency domain of the molecules at same time. Most importantly the properties of the solutions at equilibrium and also flow rate and diffusion pattern of the particles etc.

The process of sample purification from dust particles has been significantly improved. Passing samples over different kinds of filters of micrometer level eliminates impurities and dust effect. These advancements in LLS make it a precise instrument of spectroscopy for the micro molecular characterization of gels, polymers and composites. A constant angle for scattering is used in DLLS [49].

In DLS the light scattering is not in a perfect elastic method but it is quasi-elastically scattered, it may also be named as QELS. DLS is capable of obtaining information about intensity and correlation of variation. Brownian motion of molecule contributes to the variation in intensity. The path followed by the molecules may be

drawn by using the scattered light intensity; these results are obtained experimentally and theoretically. For the degree of the fluctuations in the intensity Fast photon counter [50] is used from scattered light dependent on time.

The fluctuations in intensity are due to Brownian and there is a change in between distance among particles. Within a solution all particles have same probability for movement in all directions. This results in spectrum broadening. The molecular random motions in solution contribute into a Doppler Shift that in turn changes wavelength of the incident light. The shift in frequency of radiation scattered to lower or upper values because of speed and direction is due to Doppler Effect [51].

2.4 X-Ray Diffraction (XRD)

Solid matter can be described as,

(a) Amorphous Solid:

The solid in which there is no regular pattern inside the particles is called amorphous solid e.g. glasses are amorphous solid.

(b) Crystalline Solid:

The solid in which there is a regular pattern inside the particles or molecules is called crystalline solid e.g. a brick in which the particles are in regular pattern in all three dimensions. The three axes may be described as a, b; c and the three angles between them are alpha, beta and gamma. About 95 percent of all solids are crystalline.

In this technique when the beam of x-rays hits the atom the electrons which are present in the atom start oscillation with the same frequency as the incoming beam. In all directions the destructive interference start and the combining waves are out of phase and this gives us no result. But when the x-rays beam hits the crystals inside the atom the electrons start oscillation with the same frequency as the incoming beam but these show constructive interference because all the crystals are arranged in regular pattern and they give us the result in form of peak.

2.4.1 Diffraction and the Bragg Equation

According to Bragg crystal planes act as mirrors. When the path difference between the two reflected beams in (a) = $n\lambda$ then constructive interference is observed.

The path difference in (a) is 2my. Since $my/d = \sin\theta$ $2my = 2d\sin\theta = n\lambda$ where “d” is the

interplanar spacing.

2.4.2 Scherrer's Formula

The following formula is used to calculate the thickness of crystallite.

$$t = \frac{K^{*}\lambda}{B^{*}cos\Theta_{B}}$$

Where "*t*" thickness of crystallite, "*K*" constant dependent on crystallite shape (0.89), "λ" x-ray wavelength, "*B"* FWHM (full width at half max) or integral breadth, "*Θ"* Bragg angle, "*B"* (2*θ* High) – (2*θ* Low) and "*B"* is the difference in angles at half max.

2.5 Scanning Electron Microscopy (SEM)

SEM used focused electrons beam that produces images of a sample by scanning. The electrons interact with atoms in the sample, producing various signals that can be detected and that contain information about the sample's surface, composition etc. SEM can achieve resolution better than 1 nanometer. Specimens can be observed in high vacuum, in low vacuum, in wet conditions (in environmental SEM), and at a wide range of cryogenic or elevated temperatures.

The most common SEM mode is detection of secondary electrons emitted by atoms excited by the electron beam. The number of secondary electrons depends on the angle at which beam meets surface of specimen. By scanning the sample and collecting the secondary electrons with a special detector, an image displaying the topography of the surface is created.

Chapter-3
Experimental

3.1 Chemicals Used

2-Hydroxyethyl methacrylate (HEMA) (0.5mM, 0.067ml), Methacrylic acid (MAA) (1.5mM, 0.1404ml), N-isopropylacrylamid (NIPAM) (7.5mM, 0.934g), N,N-Methylenebisacrylamide (MBA) (0.5mM, 0.0845g) were purified by recrystallization and distillation to remove the inhibitors before use. Ammonium persulphate (APS), Silver nitrate ($AgNO_3$), Cholorauric acid ($HAuCl_4.6H_2O$), Sodium borohydride ($NaBH_4$), 4-Nitrophenol (4-NP), Congo red (CR), Methylene blue (MB) and Eosin Y (EY) dyes were used as received. All the reactions were carried out in pure deionized water. All the materials with their abbreviations, molar masses and suppliers are given in **Table 3.1.**

Table 3.1. Used materials with their abbreviations, molar masses and suppliers

Sr. No	Name	Abbreviation	Molecular weight(g/mol)	Supplier
1	N-isopropylacrylamid	NIPAM	113.15	Aldrich
2	Methacrylic acid	MAA	100.12	Aldrich
3	2-Hydroxyethyl methacrylate	HEMA	130.14	Aldrich
4	N,N-Methylenebisacrylamide	MBA	154.17	Fluka
5	Sodium Dodecyl Sulphate	SDS	288.37	Fluka
6	Ammonium persulphate	APS	228.18	Aldrich
7	Silver nitrate	$AgNO_3$	169.87	Aldrich
8	Cholorauric acid	$HAuCl_4.6H_2O$	239.876	Aldrich
9	Sodium borohydride	$NaBH_4$	37.83	Aldrich
10	4-Nitrophenol	4-NP	139.11	Aldrich
11	Congo red	CR	696.665	Merck
12	Methylene blue	MB	319.85	Merck
13	Eosin Y	EY	691.85	Merck

3.2 Synthesis of pure Microgel

Pure ter-copolymer microgel was synthesized through free radical emulsion polymerization. All the concerned monomers i.e HEMA, MAA and NIPAM, with cross-linker MBA and surfactant SDS were put in three necked round bottom flask containing 100ml water. The mixture was stirred for 1 hour and connected with condenser, thermometer and nitrogen inlet. The solution mixture was heated to 70ºC with continuous purging of nitrogen gas. After 30 minutes 5ml of initiator, APS with concentration 0.06M was added to the solution. The color of solution was changed from transparent to milky white within 20 minutes. The reaction was continued for 6 hours to complete polymerization. The synthesized microgel was purified from impurities and unreacted monomers by decantation, and dialyzed against pure deionized water for one week with change water twice a day. The microgel was collected, dried and coded as P01 and stored for further use. A general mechanism is shown in **Figure 3.1.**

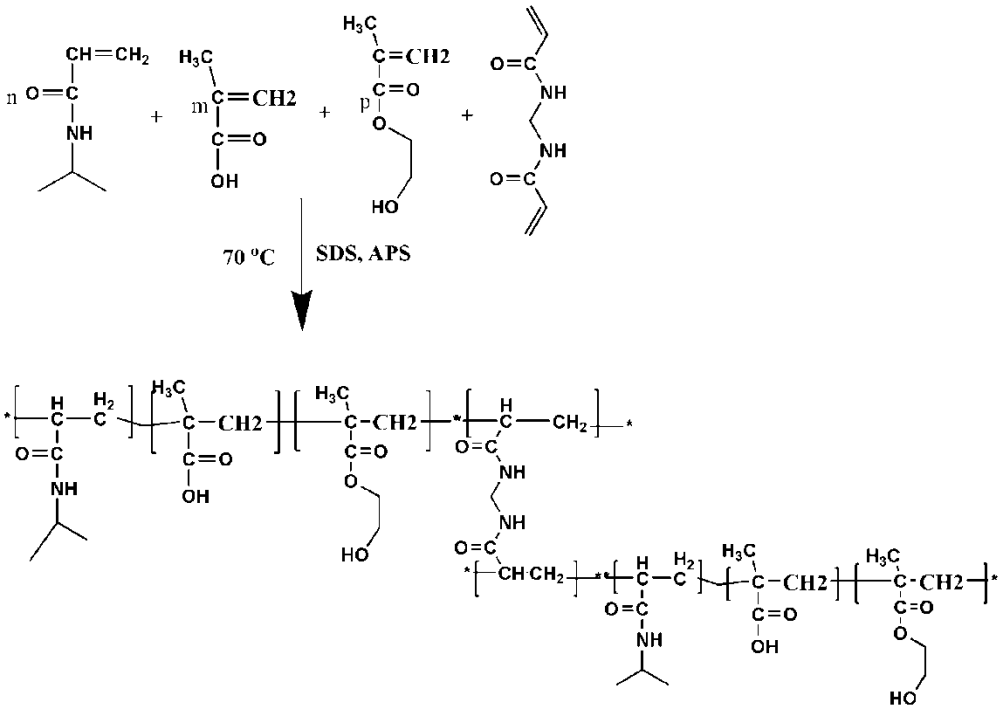

Figure 3.1 Mechanism for the synthesis of ter-copolymer microgel

3.3 Synthesis of Hybrid Microgels

Silver and gold based hybrid microgels were synthesized by insitu chemical reduction method using $NaBH_4$ as a reducing agent, at temperature 10º C and 40 ºC.

3.3.1 Synthesis of P01-Ag10 and P01-Ag40

10ml of the synthesized pure microgel was diluted by addition of 30ml of water and stirred for 2 hours. The solution temperature was adjusted to 10 ^{o}C and charged with 5ml of 0.1mM solution of $AgNO_3$ and stirred for another 01 hour in inert atmosphere. 5ml of $NaBH_4$ solution (0.2g/5ml H_2O) was added drop wise to the solution and reaction was lift for 04 hours. After completion of reaction the hybrid microgel was purified by dialysis for 03 hours, dried and coded as P01-Ag10. Hybrid microgel, P01-Ag40 was synthesized with the same procedure at 40 ^{o}C.

3.3.2 Synthesis of P01-Au10 and P01-Au40

P01-Au10 was synthesized at 10 ^{o}C by diluting the 10ml of prepared pure microgel to 40ml, the solution was stirred for 02 hours and then charged with 5ml of 0.1mM of $HAuCl_4.6H_2O$ solution, and lift the mixture for 01 hours stirring under nitrogen purging. 5ml of $NaBH_4$ solution (0.2g/5ml H_2O) was added drop wise to the solution for the complete conversion of metal ions to metal atoms. After 04 hours the reaction was stopped, the synthesized materials was purified by dialysis, dried and stored for further use. The same procedure was followed for the synthesis of P01-Au40 at 40 ^{o}C.

3.4 Catalytic Activity

The prepared hybrid microgels were used as a catalyst for the reduction of 4-nitrophenol to 4-aminophenol and for the degradation of organic dyes i.e. Methylene blue (MB), Congo red (CR) and Eosine Y (EY). 0.2mg of each specie was dissolved in 100ml of deionized water stirred for a while to form a homogeneous solution. 0.2g of reducing agent $NaBH_4$ and 0.1ml of catalyst were added to the prepared solution. The reduction process was monitored by using UV-visible spectroscopy.

Chapter-4
Results and Discussion

4.1 Fourier Transform Infrared (FTIR) Spectroscopic Study

The synthesis of both pure and hybrid microgels were confirmed by using FTIR technique. The FTIR spectra for P01, P01-Ag10 and P01-Au10 are given in **Figure 4.1**. The disappearance of strong peaks in the range of 500 to 990 cm^{-1} confirms the polymerization of vinyl groups present in monomers. The broadness of the N-H stretching peak at 3500 cm^{-1} is due to the presence of H-bonding between hydrophilic part of polymer chains and water molecules, which indicates the microgel formation. The peak at 1642 cm^{-1} is due to the carbonyl group of amide. The presence of silver and gold nanoparticles inside the polymer network was also confirmed by FTIR study. For P01-Ag10, a slight red shift to 1649 cm^{-1} observed in the FTIR spectrum shown in **Figure 4.1** is due to the interaction between Ag NPs and carbonyl group. Similar shift was also observed for P01-Au10 given in **Figure 4.1.** For P01-Au10 the shift is more as compared to P01-Ag10. This is because of the small size and strong interaction of Au NPs with carbonyl groups compared to Ag NPs.

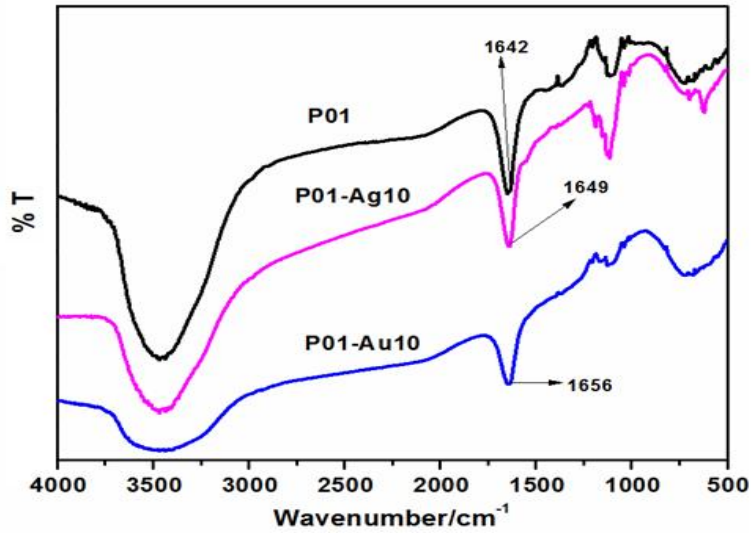

Figure 4.1.FT-IR spectra forP01, P01-Ag10 and P01-Au10 microgels

4.2 Dynamic Laser Light Scattering (DLLS)

4.2.1 Effect of pH on particle size

Due to the presence of pH sensitive MAA moiety, the ter-copolymer microgel shows the pH responsive behavior. The pH effect on particle size was studied at the entire pH range from 2 to 10 using DLS. It was found that with the increase in pH, the particles size enhanced. This change in size is due to the protonation and deprotonation of the carboxyl groups. When pH of the medium is less than the pKa value of MAA i.e. 4.3 the carboxyl groups exist in protonated form and as a result particles size reduced. pH value high than 4.3 causes deprotonation of the carboxyl groups which produced strong repulsive forces inside the microgel network, due to which particles size increases. The effect of pH change on particle size of microgel is given in **Figure 4.2.**

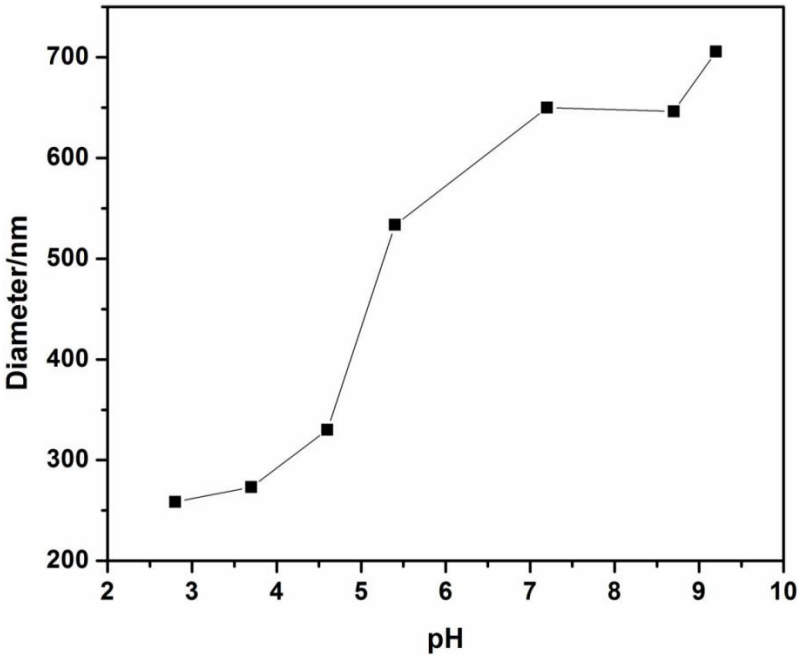

Figure.4.2 Plot of hydrodynamic diameter as a function of pH for P01 at temperature 25^{o}C

4.2.2 Effect of Temperature on Particle Size

The presence of temperature sensitive segment PNIPAM, introduces thermo responsive behavior in polymer microgel. The temperature effect on particle size was evaluated at pH 2.6 and 8.5.

At pH 2.6, the increase in temperature causes reduction in the particle size. This reduction in size is due to the expelling of water molecules from polymer network, by

breaking of H-bonding between water molecules and polymer chains with the increase in temperature. After 45 °C, the size of particles become constant showing the poor solvent behavior of water at high temperature, results are explored in **Figure 4.3.**

At pH 8.5, no effect of temperature on particle size was observed in the entire experimental range as shown in **Figure 4.4.** This is because of the existence of carboxyl groups in deprotonated form, which produces repulsive columbic forces in the network due to which the particles cannot shrink.

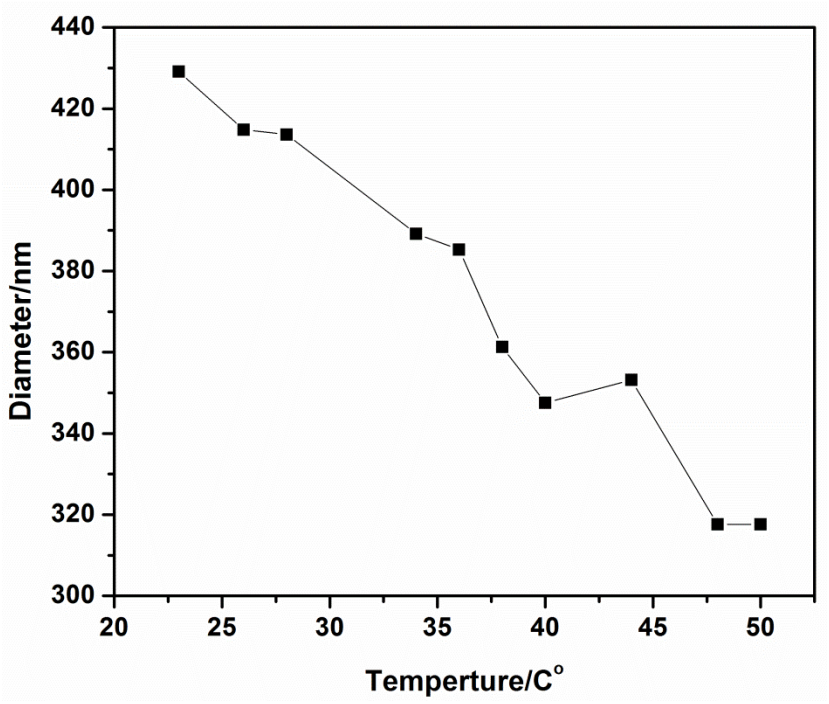

Figure 4.3.Temperature effect on particle size for P01 at pH 2.6

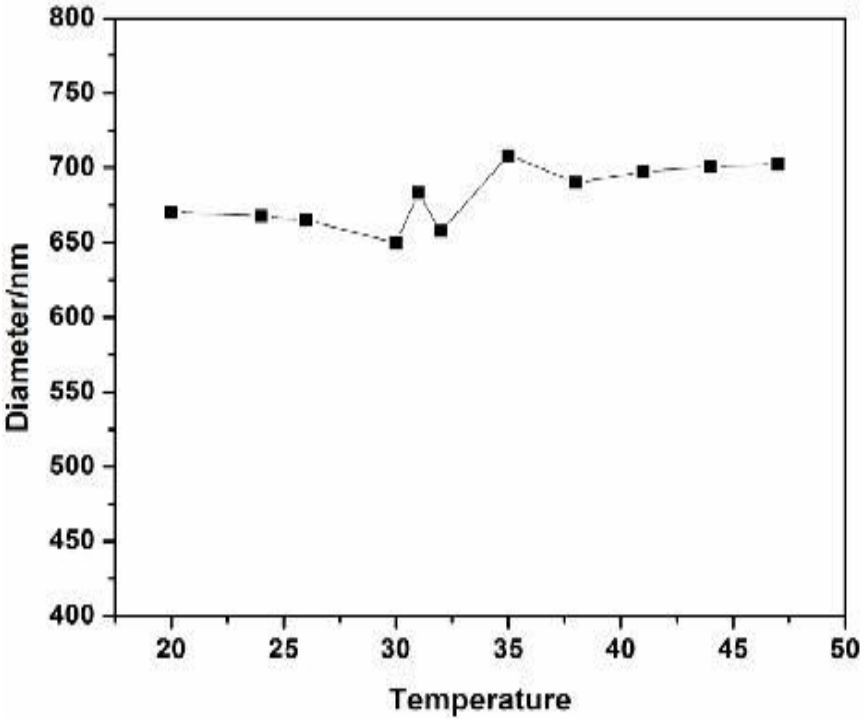

Figure 4.4. Temperature effect on particle size for P01 at pH 8.5

4.3 Scanning Electron Microscopy (SEM)

The morphology and size of pure and hybrid microgels were investigated by scanning electron microscopy (SEM). The **Figure 4.5** shows a typical SEM image of P01, the size obtained is 250nm which is lower than the size value obtained by DLS. This is because of the fact that SEM calculates the size in dry state while DLS calculate the size in solution form. **Figure 4.6** shows the SEM image of P01-Au40, Au nanoparticles indicated by small black dots in the image embedded in the polymer matrix without forming any aggregation of particles. This shows that polymer microgel can be used as a good stabilizer for the metal nanoparticles. The SEM image of P01-Ag40 is given in **Figure 4.7.** The size for Ag nanoparticles was found greater than Au nanoparticles.

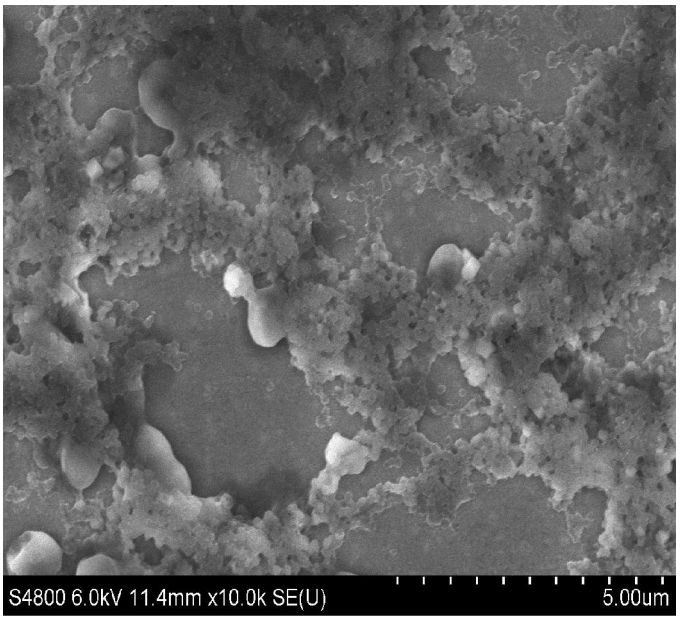

Figure.4.5. SEM image of P01

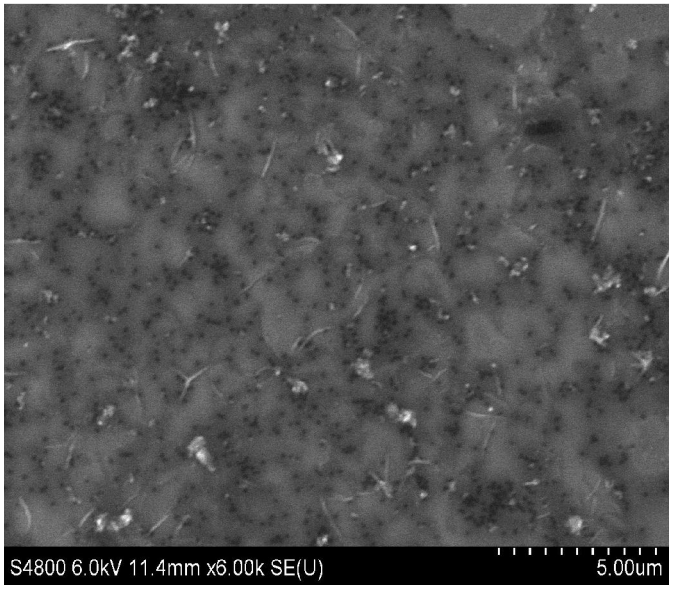

Figure 4.6.SEM image of P01-Au40

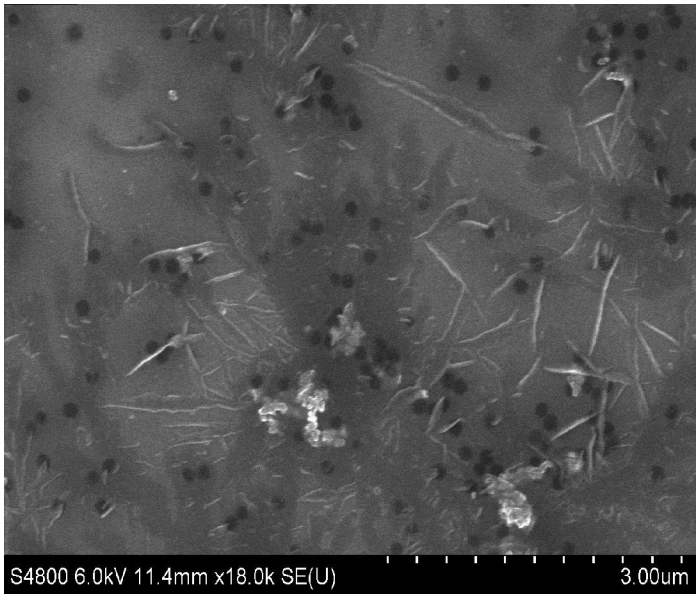

Figure 4.7SEM image of P01-Ag-40

4.4 X-Rays Diffraction (XRD)

Figure 4.8 displays the X-ray diffraction (XRD) spectra of P01, P01-Ag10 and P01-Au10. P01 spectrum shows the broad peak indicates the amorphous nature of pure microgel.

The XRD spectrum for P01-Ag10 shows all the corresponded reflections to Ag with face-centered cubic (FCC) symmetry. The reflections were indexed as (111), (200) and (220), (311) and (222) with the corresponding 2Θ values of 23.1, 34.11, 47.27, 54.42, and 75.1 respectively. The intensity of the peaks reveals the degree of crystallinity of the Ag nanoparticles. Similarly, the peaks observed in P01-Au. The reflections were indexed as (220), (311) and (111), (400) and (440) with the corresponding 2Θ values of 23.1, 29.11, 31.27, 35.42, and 48.1 respectively. The intensity of the peaks reflects the degree of crystallinity of the Au nanoparticles.

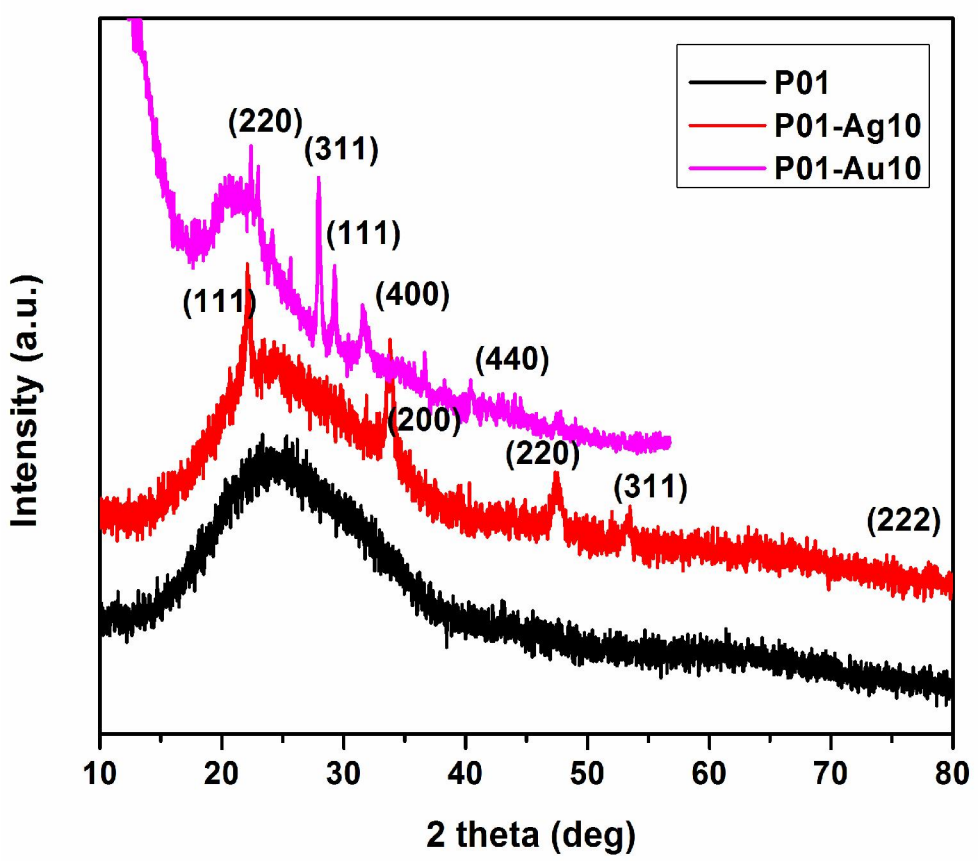

Figure 4.8.XRD Spectra of pure and hybrid microgels

4.5 UV-Visible Spectroscopic Study

The effect of pH and temperature on hybrid microgels was studied by investigated surface plasmon resonance (SPR) behavior of Ag and Au nanoparticles using UV-visible spectroscopy.

4.5.1 Effect of pH on SPR for P01-Ag40 and P01-Au40

Effect of pH on SPR was studied for P01-Ag40 and P01-Au40. The appearance of peak at 400nm indicates the existence of Ag nanoparticles inside the polymer network. It was found that by increasing pH of the medium a blue shift and decrease in absorption intensity occurs as shown in **Figure 4.9.** The shift is concerned with inter particles coupling, which occurs due to the change in size of microgel particles. At low pH microgel particles changed into collapsed state which causes inter particles coupling of Ag nanoparticles and produced a red shift. When we increase pH, the microgel particles changes into swollen state, as a result the metal particles go far apart from each other and a blue shift takes place.

The effect of pH on SPR for P01-Au40 also gives the same results. The characteristic peak at 520nm confirms the formation and existing of Au nanoparticles inside the polymer network. The increase in pH produces a blue shift and increase in absorption intensity due to inter particles coupling of Au nanoparticles, with changing the size of microgel particles by pH change. The results are given in **Figure 4.10.**

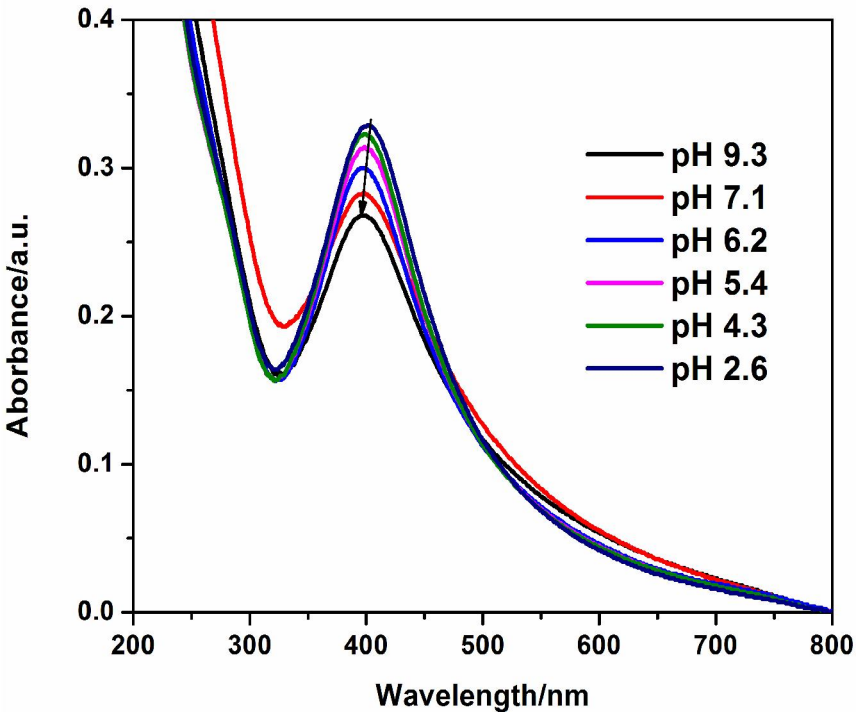

Figure 4.9.pH effect on SPR for P01-Ag40

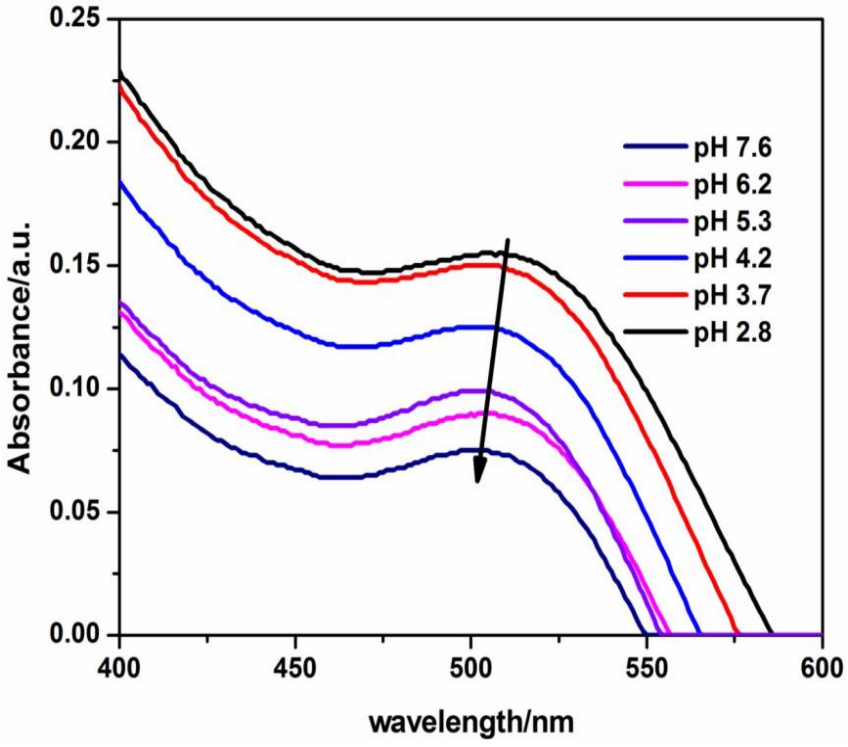

Figure 4.10.pH effect on SPR for P01-Au40

4.5.2 Effect of Temperature on SPR for P01-Ag40 and P01-Au40

Temperature effect on SPR was studied for P01-Ag40 and P01-Au40 at pH 2.6 and 8.2. The increase in temperature at pH 2.6 causes a red shift and increase in absorption of both P01-Ag40 and P01-Au40 hybrid microgels. This is due to the shrinkage of polymer network with increase in temperature, which produced inter particles coupling and also increase the refractive index inside the polymer network compared to outside of the solvent. The results are given in **Figure 4.11** and **Figure 4.12** for P01-Ag40 and P01-Au40 respectively.

At pH 8.2, there is no change in SPR and absorbance value observed because at high pH, the carboxyl groups are in deprotonated form and produced strong repulsive forces inside the network, which keeps the polymer network in swollen state and temperature increase produces no effect on particle size. Therefore the SPR remained almost constant and are shown in **Figure 4.13** for P01-Ag40 in **Figure 4.14** for P01-Au40.

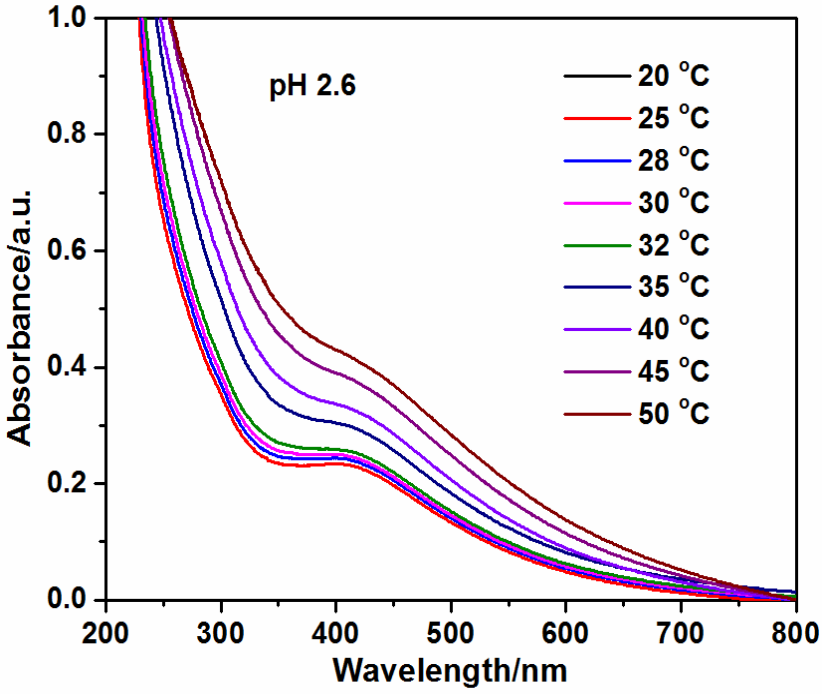

Figure.4.11. Effect of temperature on SPR for P01-Ag40 at pH 2.6

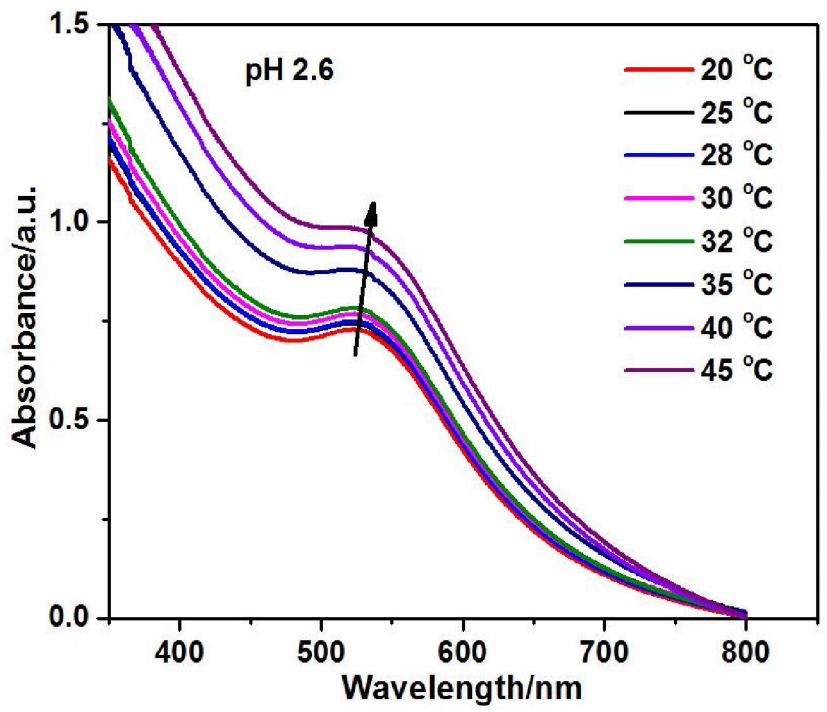

Figure.4.12. Effect of temperature on SPR for P01-Au40 at pH 2.6

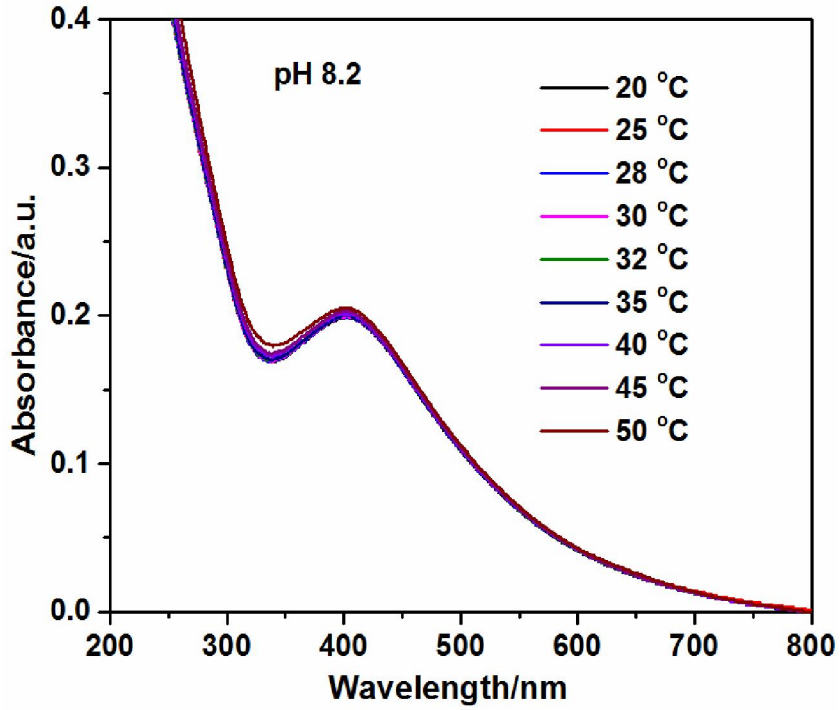

Figure 4.13. Effect of temperature on SPR peak of P01-Ag40 at pH 8.2

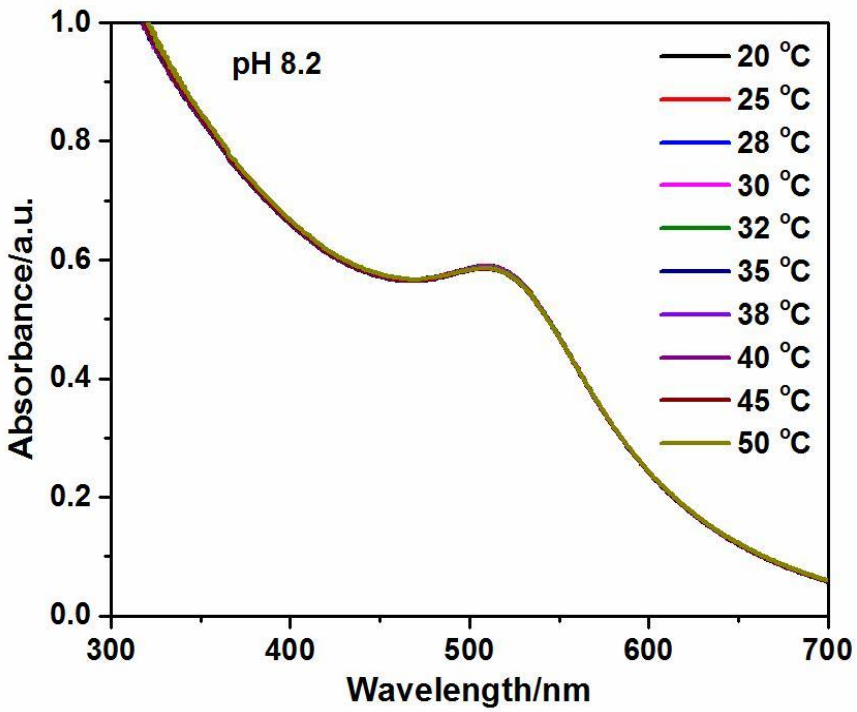

Figure.4.14. Effect of temperature on SPR peak of P01-Au40 at pH 8.2

4.6 Catalytic Activity of Hybrid Microgels

After the successful synthesis and characterization of hybrid microgels of silver and gold they were used for the conversion of 4-nitrophenol to 4-Aminophenol and for the degradation of Congo red (CR), Methylene blue (MB) and Eosine Y (EY).

4.6.1 Reduction of 4-Nitrophenol

4-nitrophenol (4-NP) is the toxic pollutant found in waste water, whereas 4-Aminophenol (4-AP) is a good material and can be used for a number of applications. Therefore we reduced 4-NP to 4-AP using $NaBH_4$ as reducing agent and hybrid microgel as a catalyst. 4-NP solution appears light yellow in color and gives a characteristic peak at 317nm, after the addition of $NaBH_4$ the color of solution changes to dark yellow due to the formation of nitrophenolate ion and the peak shifted to 400nm as shown in **Figure 4.15.** Without the addition of catalyst the solution concentration and color were stable for a long time. This indicates that the reaction is restricted kinetically. After the addition of catalyst the peak intensity at 400nm reduced with time and a new peak appeared at 300nm. Reduction in the peak at 400nm confirms the disappearance of nitrophenolate ion while the appearance of new peak at 300nm indicates the formation of 4-AP. The UV-

visible spectra obtained using P01-Ag10 as a catalyst is given in **Figure 4.15.**

The catalyst efficiency was calculated by finding the apparent rate constant (k_{app}) value obtained from the slope of the plot, made by plotting $\ln(C_t/C_o)$ against time. Where C_t is the concentration or absorbance at any time "t" and C_o is the initial absorbance of nitrophenolate ions. The reaction follows pseudo first order kinetics because the amount of reducing agent is in access compared to 4-NP, so the rate of reaction only depends on the amount of 4-NP. **Figure 4.16** shows a plot obtained for the reduction of 4-NP to 4-AP by $NaBH_4$ using P01-Ag10 as a catalyst. The rate constant value is $1.12\times10^{-3}S^{-1}$.

The same reaction was catalyzed by P01-Ag40 and results are given in **Figures 4.17** and **4.18.** The k_{app} was found to be $1.6\times10^{-3}S^{-1}$, which is greater than the value obtained for P01-Ag10. The reason for this is the formation of some Ag nanoparticles on the surface of polymer microgel, because at high temperature the microgel particles are in fully collapsed state and penetration of metal ions inside the network become difficult, so most ions reduced on the surface and increase the exposure of metal nanoparticles to reactants during reaction which increase the catalytic activity.

P01-Au10 and P01-Au40 were used as a catalyst for the same reduction process. The same trend for k_{app} was observed. The apparent rate constant value obtained for P01-Au40 is greater than for P01-Au10. The results for P01-Au10 are explored in **Figures 4.19** and **4.20**, while for P01-Au40 are presented in **Figures 4.21** and **4.22.**

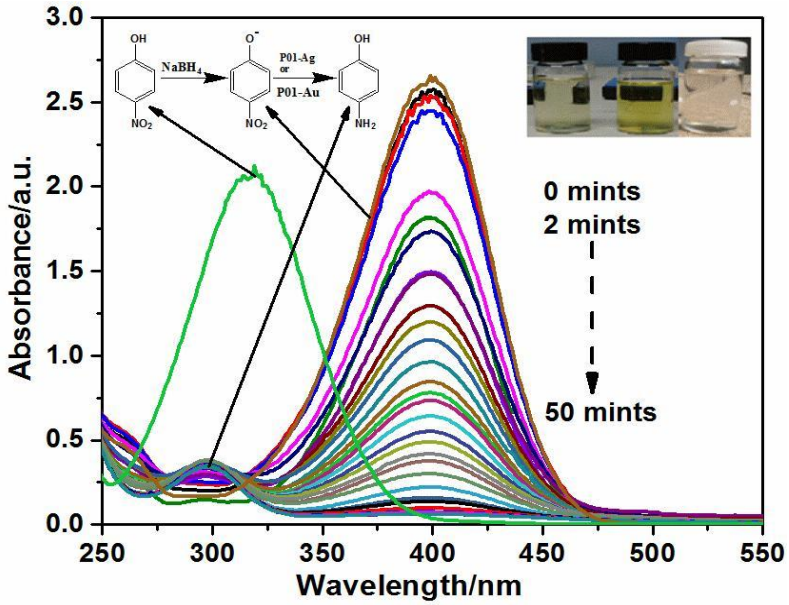

Figure 4.15.UV-vis spectra for the conversion of 4-NP into 4-AP by P01-Ag10

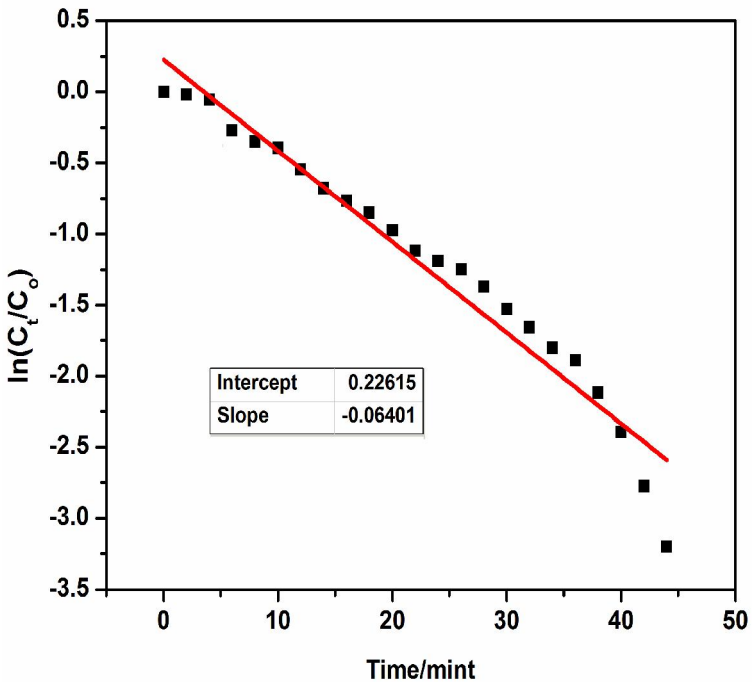

Figure 4.16 Plot of $\ln(C_t/C_o)$ vs. time for the conversion of 4-nitrophenol by P01-Ag10

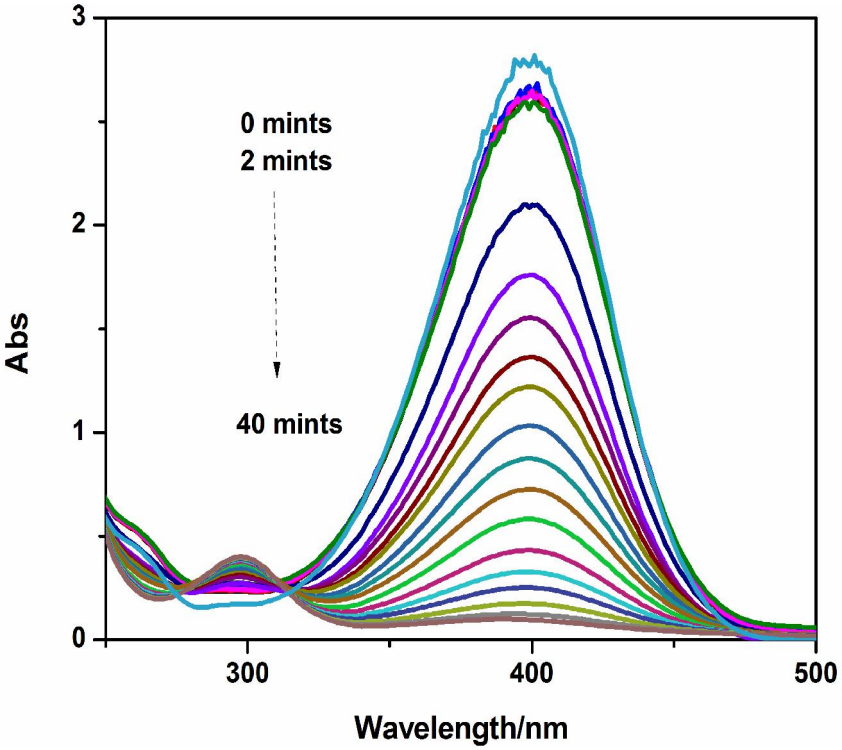

Figure 4.17.UV-vis spectra for the conversion of 4-NP into 4-AP by P01-Ag40

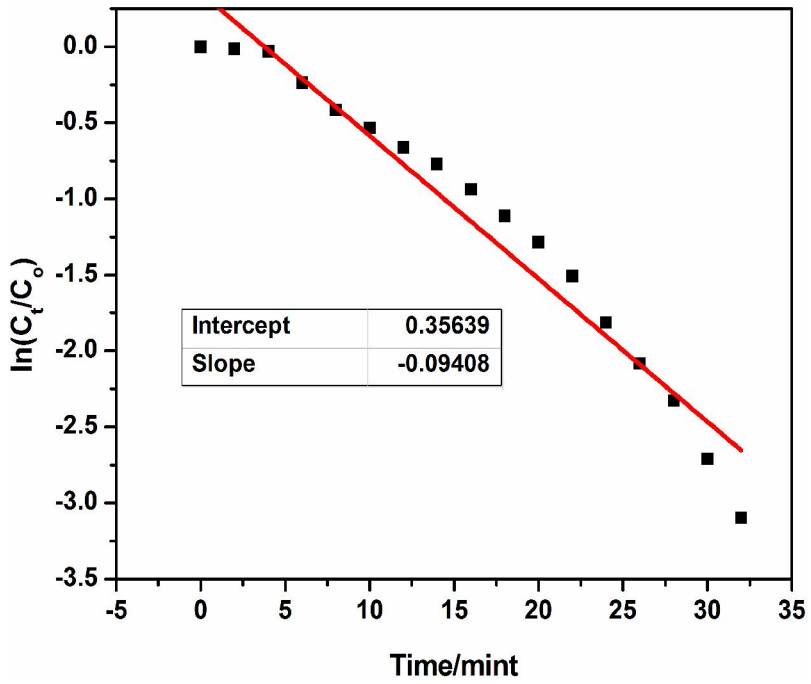

Figure 4.18 Plot of $\ln(C_t/C_o)$ vs. time for the conversion of 4-NP to 4-AP by P01-Ag40

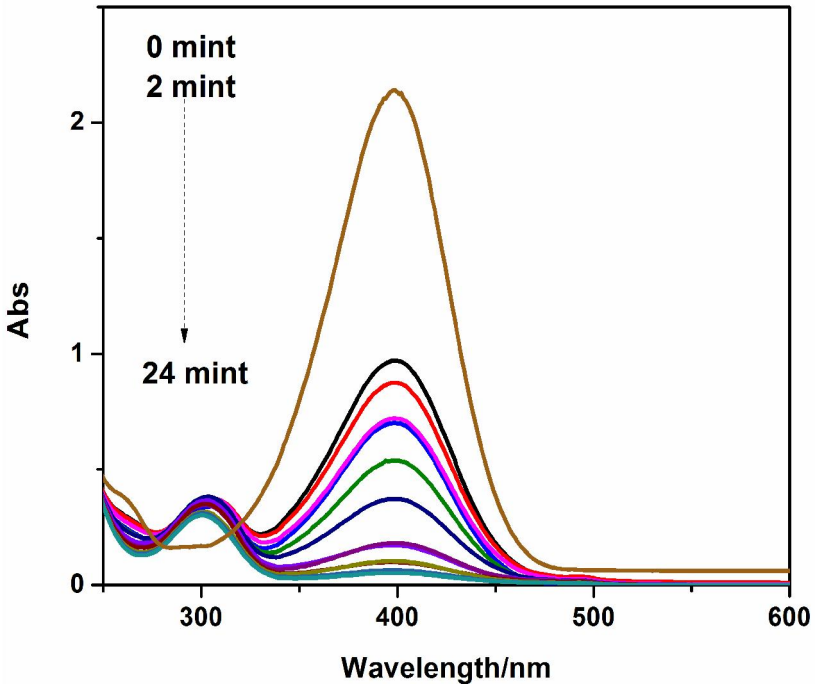

Figure 4.19.UV-vis spectra for the conversion of 4-NP to 4-AP by P01-Au10

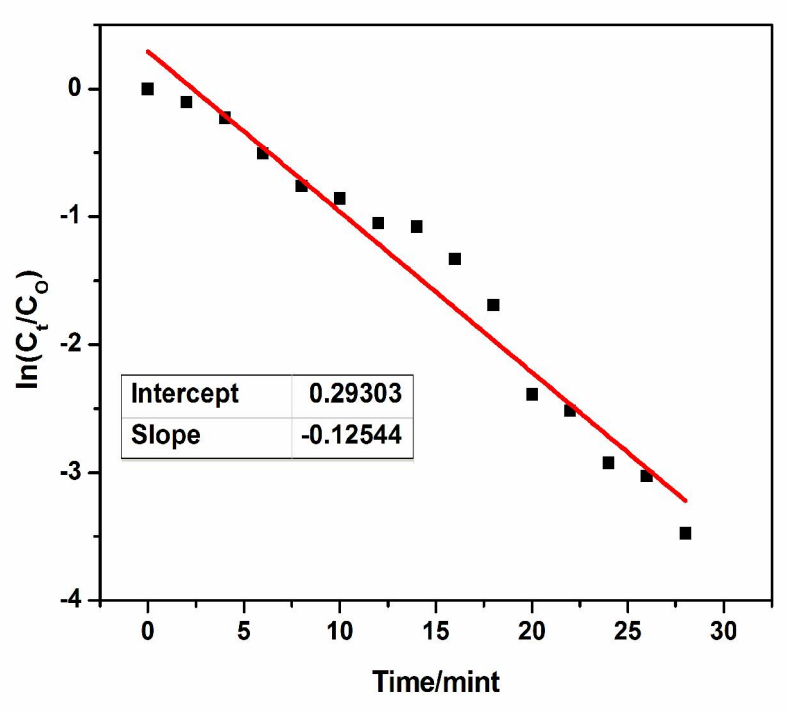

Figure 4.20.Plot of $\ln(C_t/C_o)$ vs. time for the conversion of 4-NP to 4-AP by P01-Au10

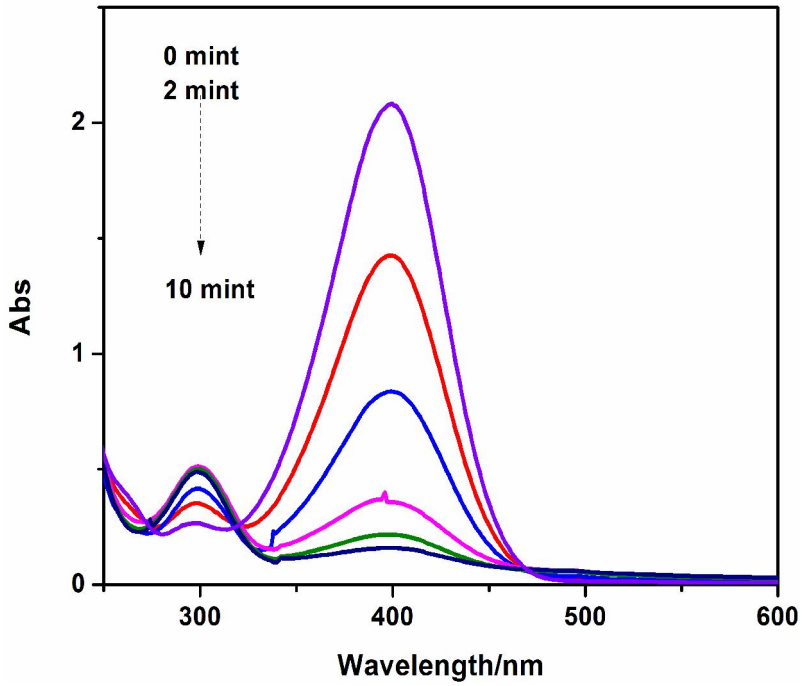

Figure 4.21.UV-vis spectra for the conversion of4-NP to 4-AP by P01-Au40

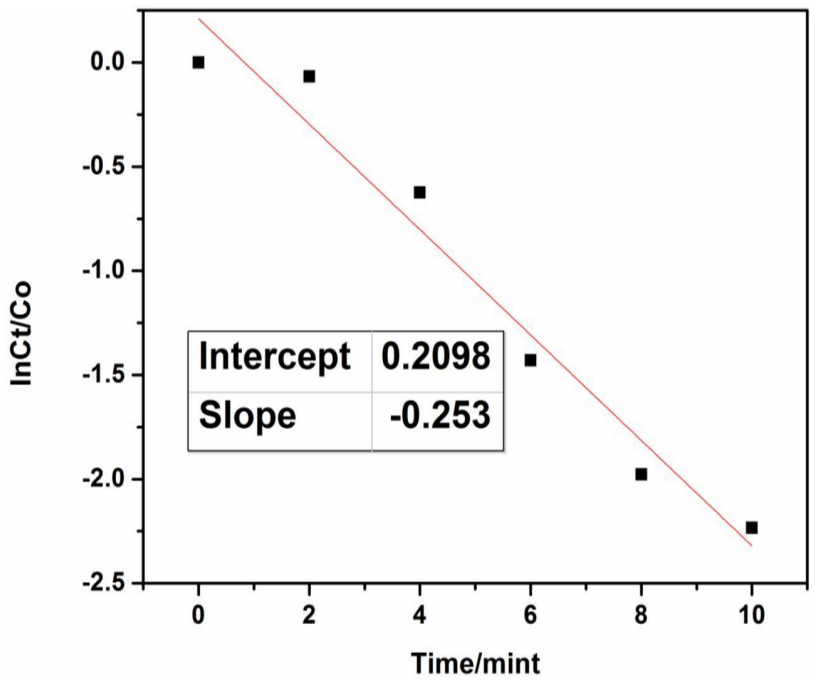

Figure 4.22.Plot of ln(C_t/C_o) vs. time for the conversion of 4-NP to 4-AP by P01-Au40

The k_{app} values for all catalysts are given in **Table 4.1**. Au based hybrid microgels were found more efficient than Ag hybrid microgels. Because the Au nanoparticles are very small having large surface area compared to silver nanoparticles with larger size.

Table 4.1: Obtained k_{app} values for all catalysts used for conversion of 4-NP to 4-AP

Catalyst used	**$k_{app}\times10^3$ S^{-1}**
P01-Ag10	1.12
P01-Ag40	1.60
P01-Au10	2.11
P01-Au40	4.22

4.6.2 Temperature Effect on Catalytic Activity

The effect of temperature on catalytic activity was studied at a temperature range of 20 to 50 °C. It was found that all the catalysts show increase in k_{app} value with increase in temperature. This increase is due to the swelling and de-swelling transition of polymer microgels which expose and suppress the metal nanoparticles for reactants. Initially the

increase in temperature causes the collapsing of microgel particles which pushes the Ag and Au nanoparticles to the surface and easily available to initiate the reaction. But after volume phase transition temperature further increase in k_{app} with temperature is due to the direct relationship of temperature with k_{app}.

The same trend of increase in k_{app} was found and is shown in **Figures 4.23, 4.24, 4.25** and **4.26** for P01-Ag10, P01-Ag40, P01-Au10 and P01-Au40 respectively.

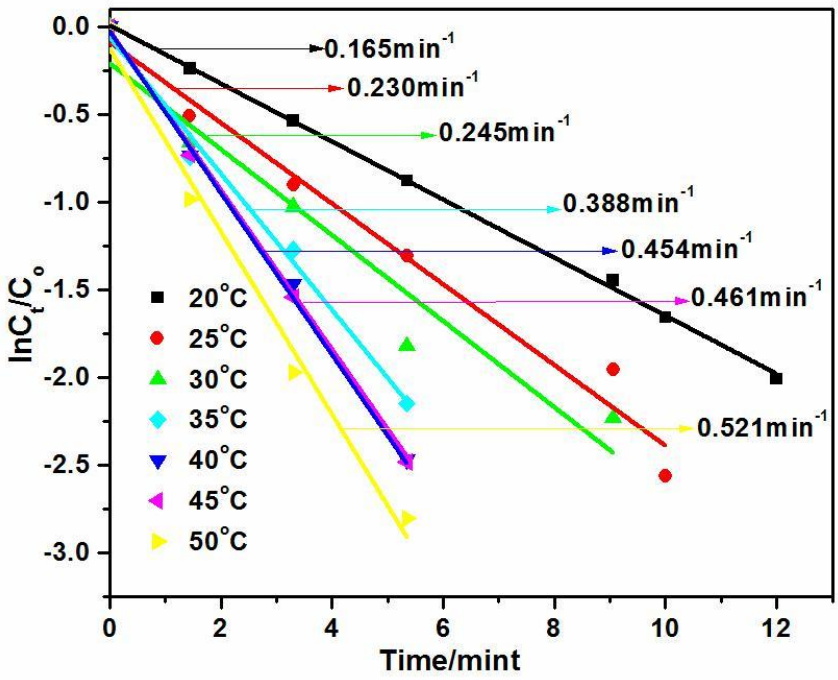

Figure 4.23.Effect of temperature on k_{app} of P01-Ag10

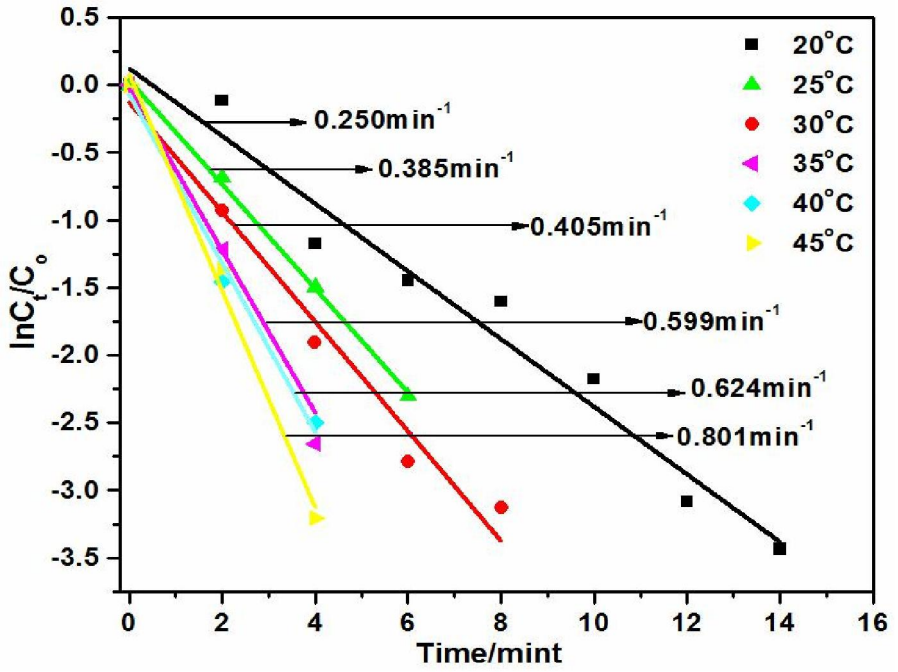

Figure 4.24. Effect of temperature on k_{app} of P01-Ag40

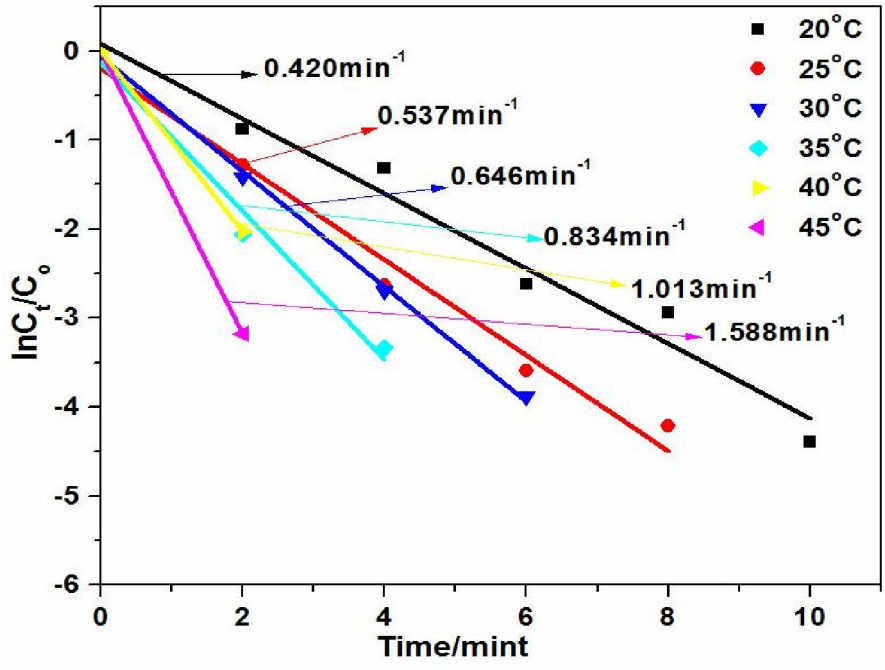

Figure 4.25. Effect of temperature on k_{app} of P01-Au10

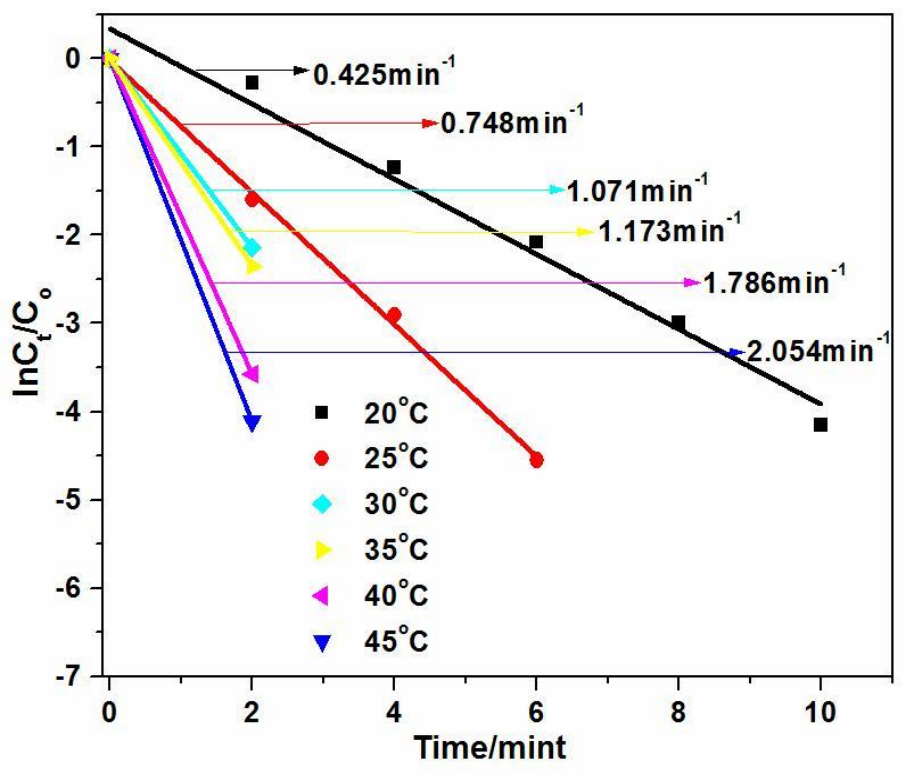

Figure.4.26.Effect of temperature on k_{app} of P01-Au40

4.7 Degradation of Dyes

The catalytic activity of the synthesized hybrid microgels were further studied for the degradation of organic dyes i.e. Congo red, Methylene blue and Eosine Y.

4.7.1 Degradation of Congo red (CR)

Congo red is a stable dye and gives red color to solution when dissolve in water, is consider as a water pollutant. It should be removed from the waste water by degrading it into other fruitful materials with reducing agent $NaBH_4$. But the reduction process is slow and takes a long time without catalyst. Here, we used the synthesized catalysts for the reduction process and results are explored in **Figures 4.27, 4.29, 4.31** and **4.33** for each catalyst. CR gives a characteristic peak at 490nm and is stable for a long time after the addition of $NaBH_4$ shows the slow reduction process. But by the addition of catalyst the peak at 490nm disappears with time and a new peak appeared at 200nm which increase in absorption intensity, indicating the successful synthesis of degraded compounds.

The catalytic activity of the used catalysts was found by calculating k_{app} values from the slope of the plot made by plotting $\ln(C_t/C_o)$ vs time. the plots obtained for P01-Ag10, P01-Ag40, P01-Au10 and P01-Au40 are given in **Figures 4.28, 4.30, 4.32** and **4.34** respectively.

Table 4.2 shows k_{app} values for all the catalysts used for the reduction of CR. The catalysts synthesized at 40 °C shows more efficiency as compared to catalysts prepared at 10 °C.

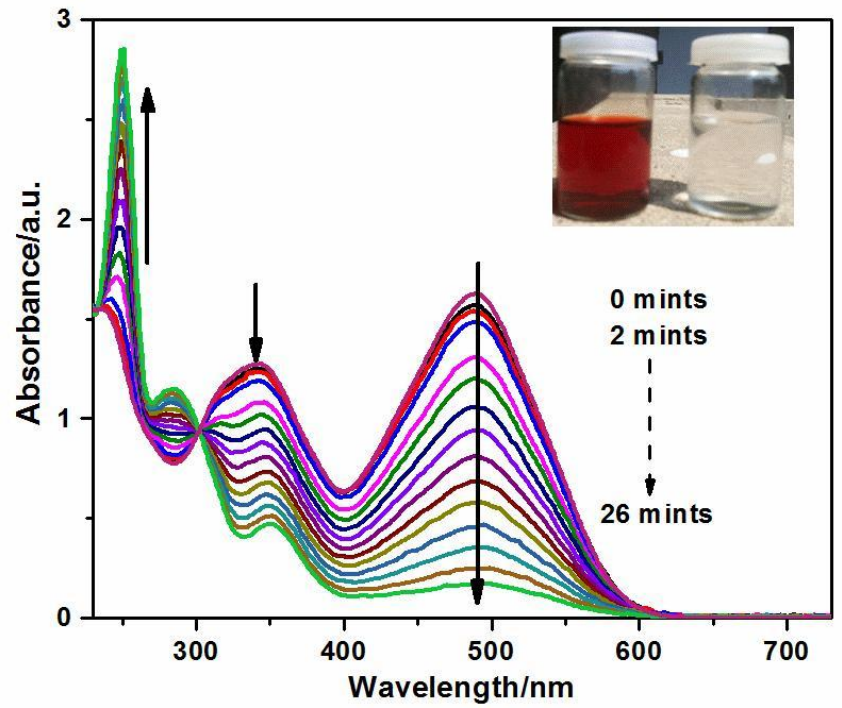

Figure 4.27.Degradation of CR through P01-Ag10

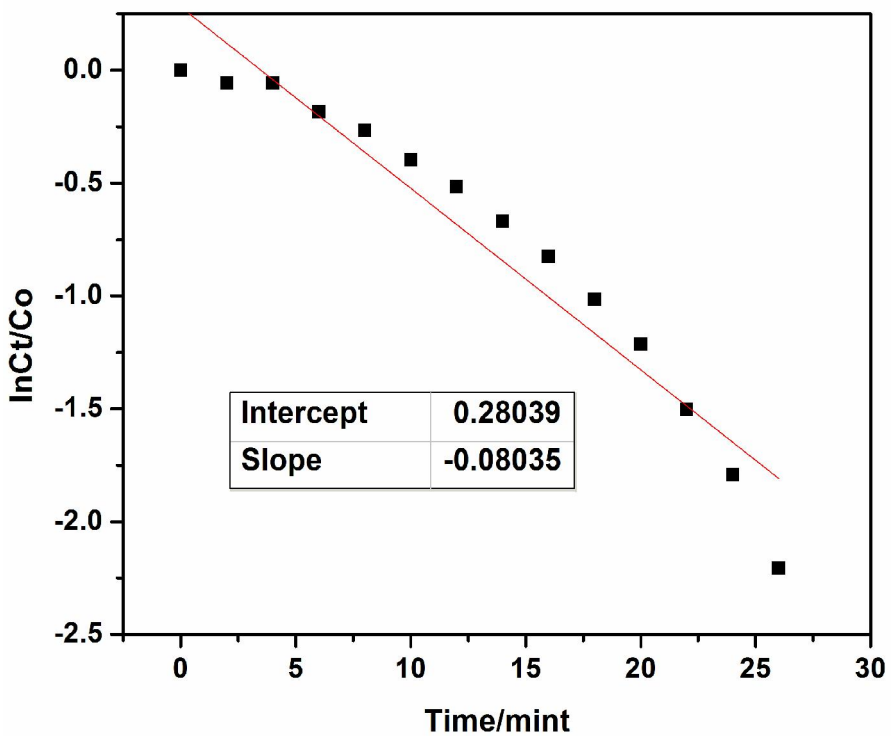

Figure.4.28. Plot of $\ln(C_t/C_o)$ vs. time for the degradation of CR by P01-Ag10

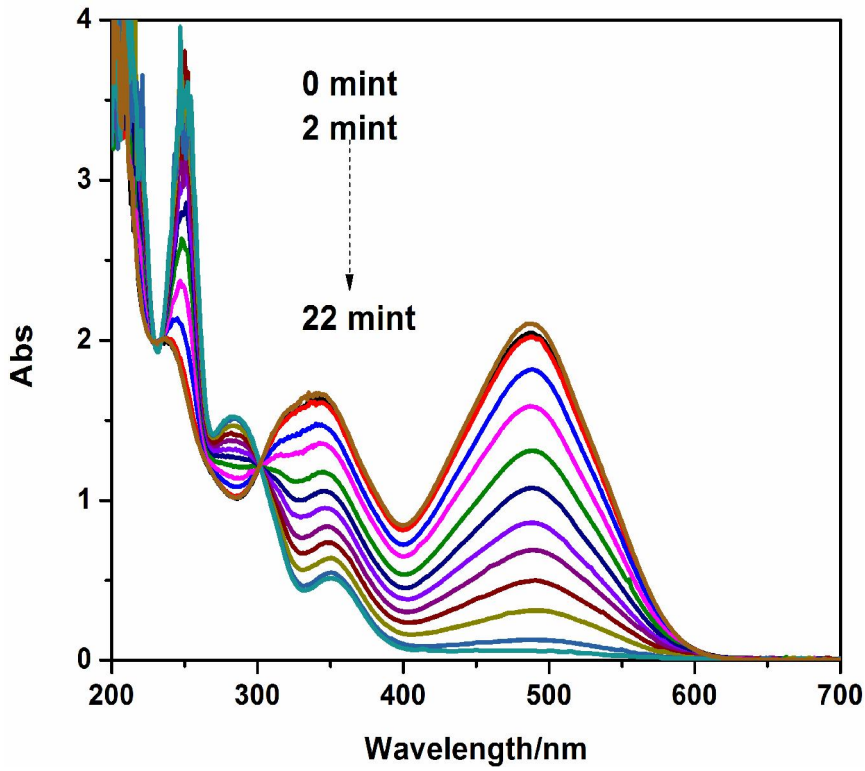

Figure.4.29. Degradation of CR through P01-Ag40

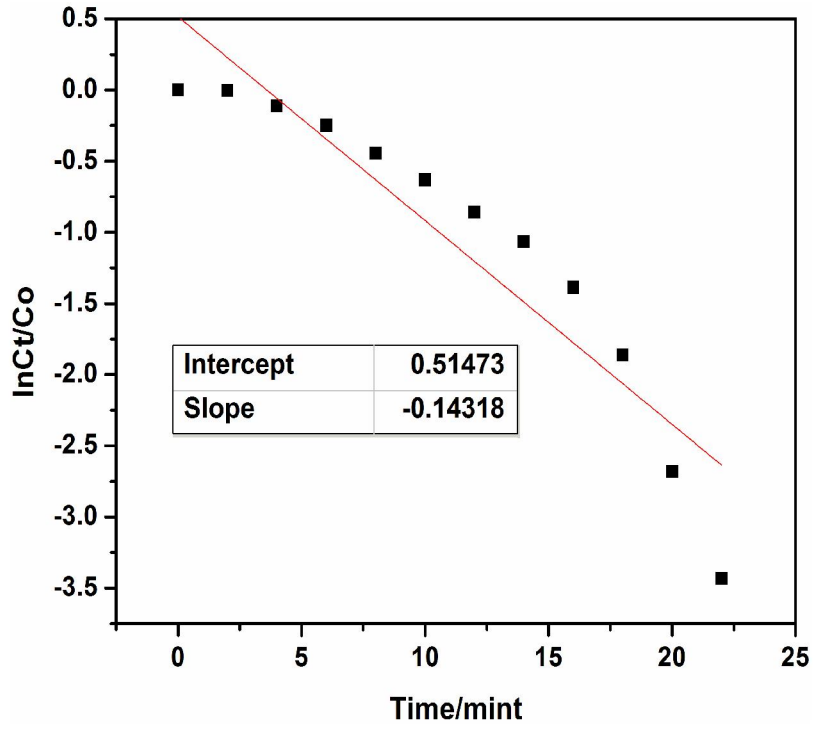

Figure.4.30. Plot of ln(Ct/Co) vs. time for the degradation of CR by P01-Ag40

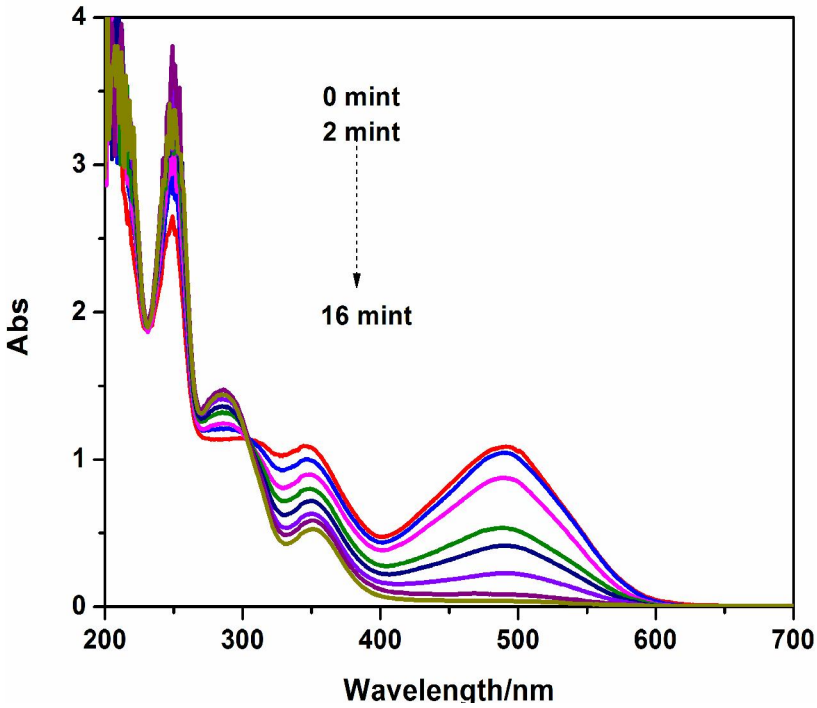

Figure 4.31. Degradation of CR through P01-Au10

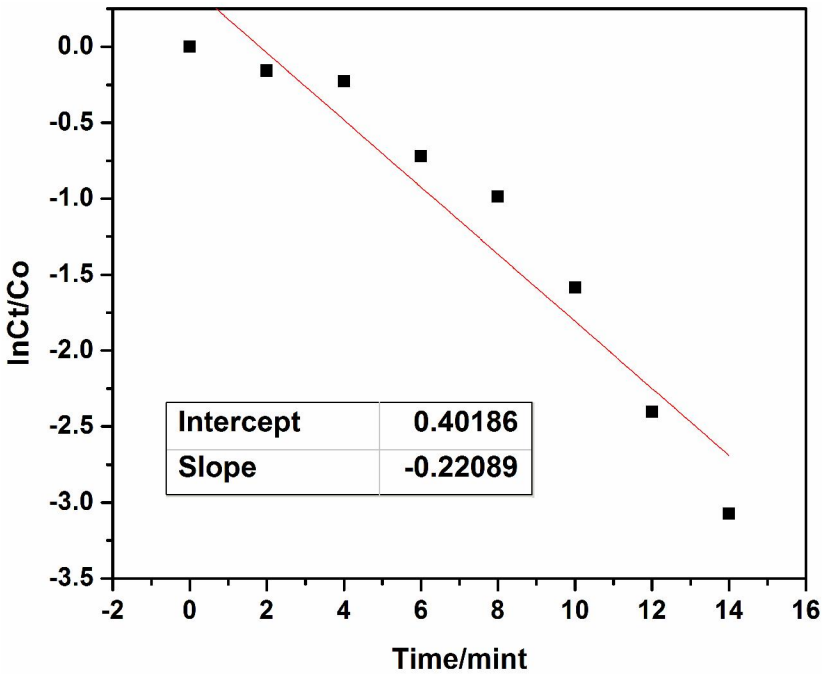

Figure.4.32.Plot of $\ln(C_t/C_o)$ vs. time for the degradation of CR by P01-Au10

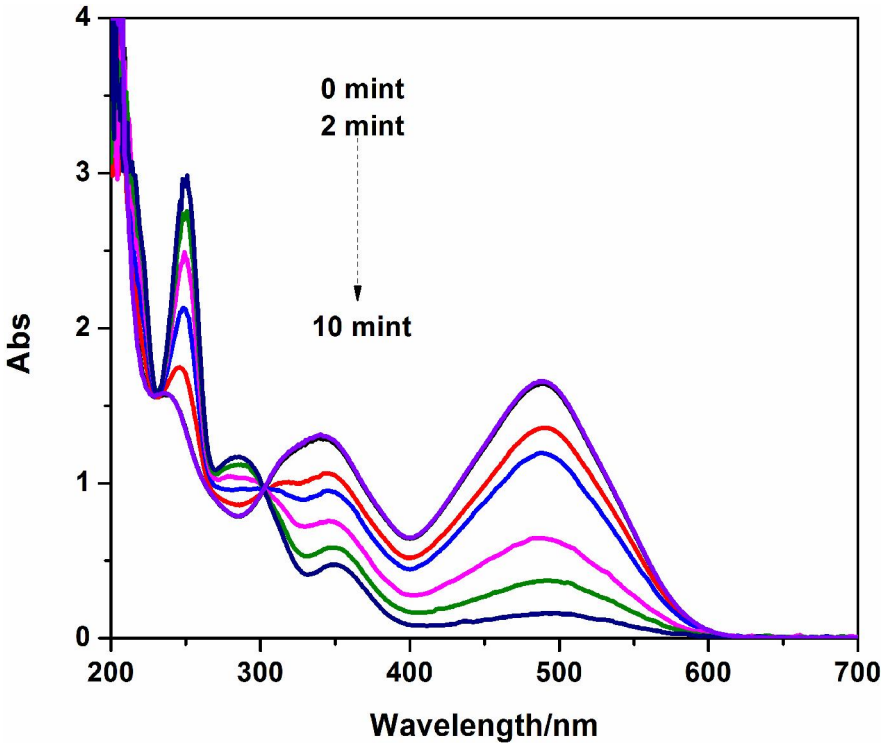

Figure.4.33. Degradation of CR through P01-Au40

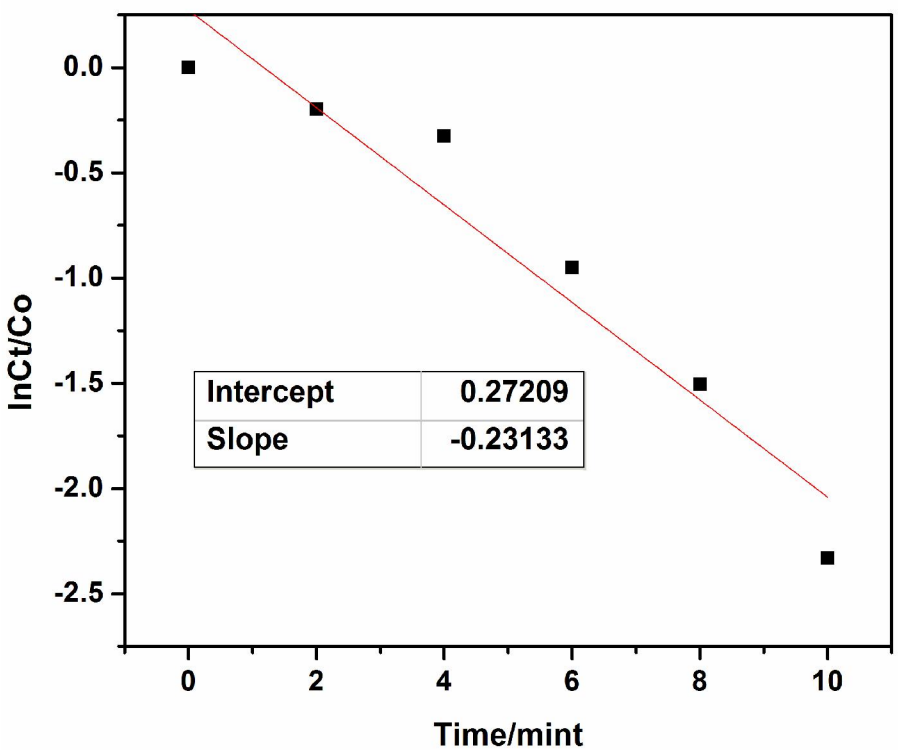

Figure.4.34. Plot of ln(C_t/C_o) vs. time for the degradation of CR by P01-Au40

Table 4.2 k_{app} values obtained for the degradation of CR

Catalyst used	$k_{app}\times10^3$ S^{-1}
P01-Ag10	1.34
P01-Ag40	2.4
P01-Au10	3.7
P01-Au40	3.9

4.7.2 Degradation of Methylene Blue (MB)

The catalysts were also applied for the degradation of Methylene blue (MB). MB solution appears blue in color with characteristic peak at 665nm, by addition of $NaBH_4$ a slight negligible reduction in the peak intensity occurs for a long time. By the application of catalyst the reduction process becomes enhanced with the decrease in absorption intensity at 665nm. The appearance and increase in peak intensity at 250nm shows the

formation of products. All the UV-visible spectra taken for the degradation of MB using P01-Ag10, P01-Ag40, P01-Au10 and P01-Au40 catalyst are given in **Figures 4.35, 4.37, 4.39** and **4.41** respectively.

The k_{app} values were calculated using pseudo first order kinetics and are tabulated in **Table 4.3**. The slope gives the k_{app} value for catalyst used in the reaction. The plots are shown in **Figures 4.36, 4.38, 4.40** and **4.42.**

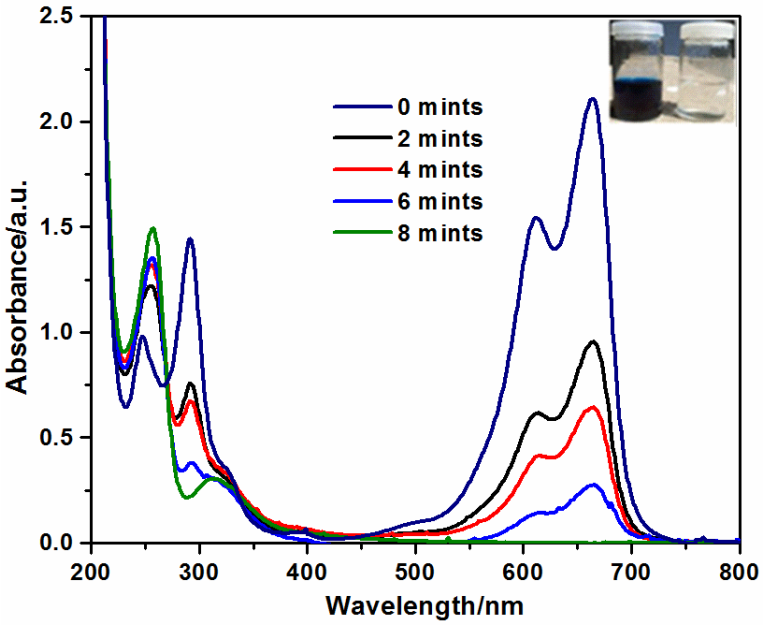

Figure.4.35. Degradation of MB through P01-Ag10

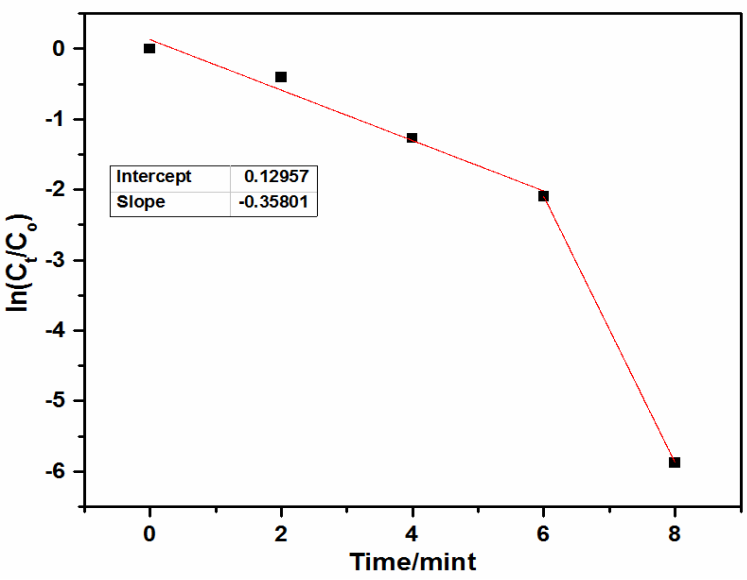

Figure.4.36. Plot of $\ln(C_t/C_o)$ vs. time for the degradation of MB by P01-Ag10

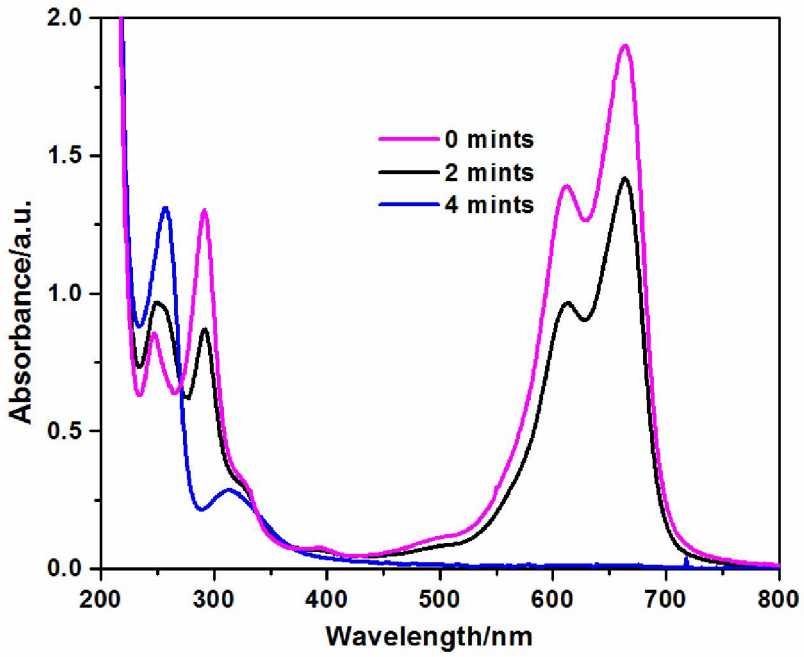

Figure.4.37. Degradation of MB through P01-Ag40

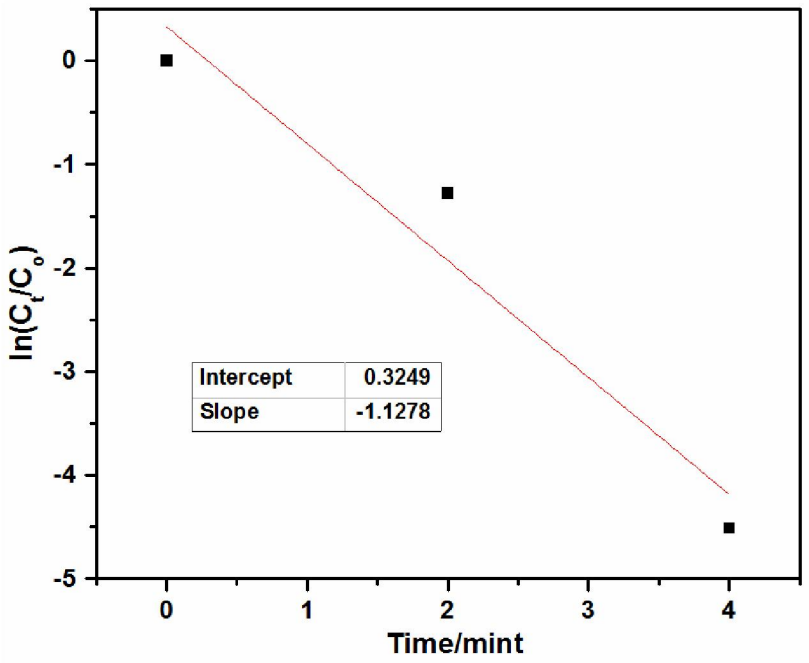

Figure.4.38. Plot of $\ln(C_t/C_o)$ vs. time for the degradation of MB by P01-Ag40

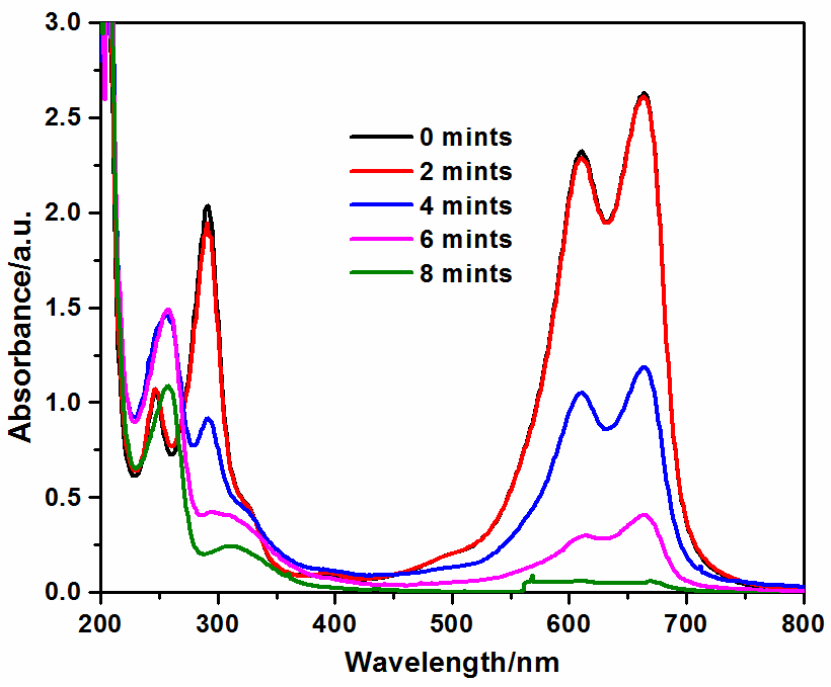

Figure.4.39. Degradation of MB through P01-Au10

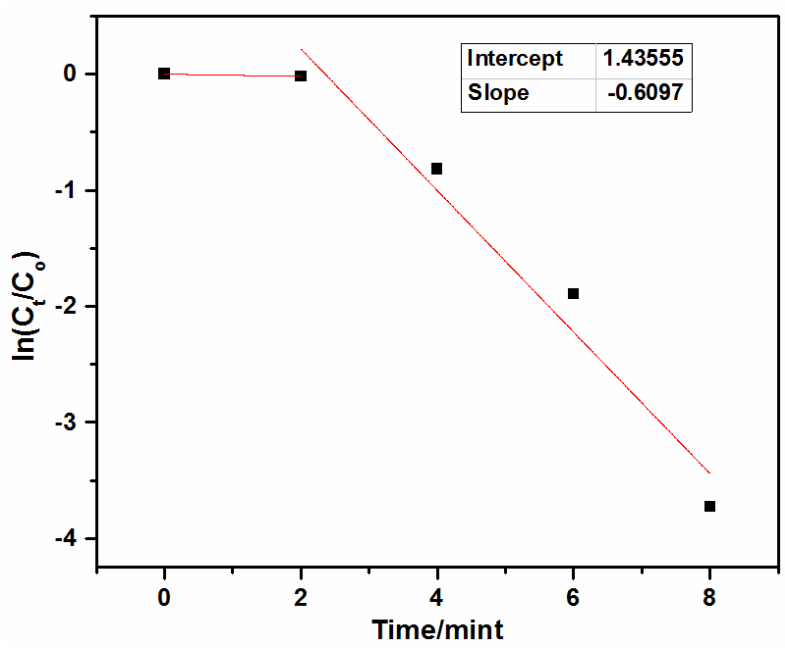

Figure.4.40. Plot of $\ln(C_t/C_o)$ vs. time for the degradation of MB by P01-Au10

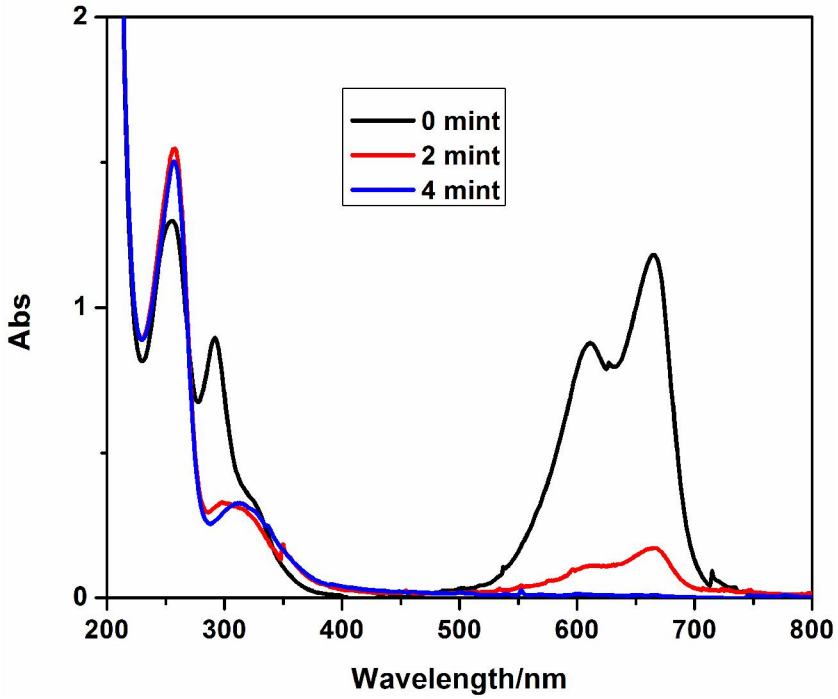

Figure.4.41. Degradation of MB through P01-Au40

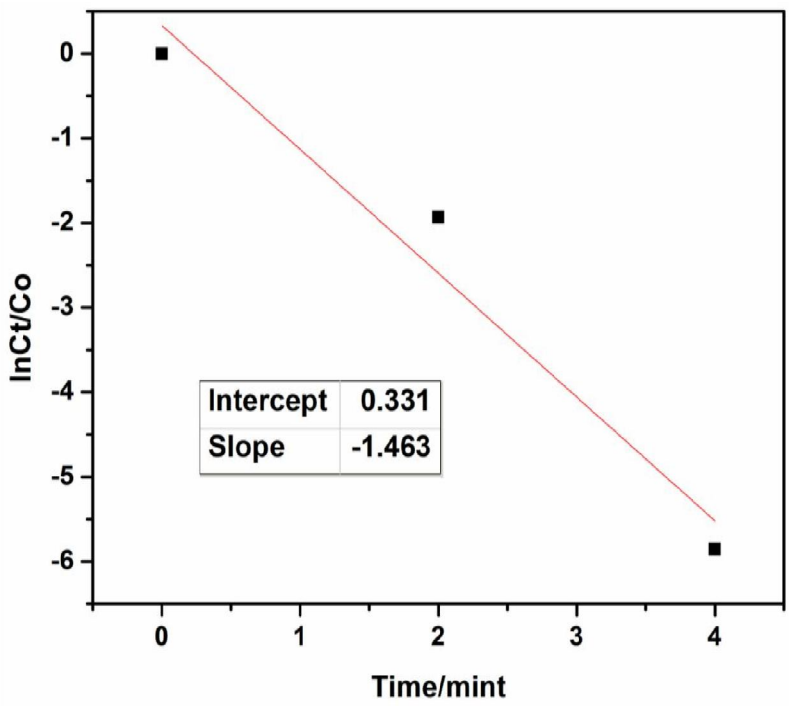

Figure.4.42. Plot of $\ln(C_t/C_o)$ vs. time for the degradation of MB by P01-Au40

Table 4.3 k_{app} values obtained for the degradation of MB

Catalyst used	$k_{app} \times 10^2$ S^{-1}
P01-Ag10	0.61
P01-Ag40	1.87
P01-Au10	1.02
P01-Au40	2.44

4.7.3 Degradation of Eosin Y (EY)

Eosin Y gives a characteristic peak at 520nm in the visible region and was reduced by $NaBH_4$ using catalyst. After the addition of catalyst the colored solution becomes colorless and the peak at 520nm disappeared and a new peak appeared at 405nm indicating the degradation of EY. The results are given in **Figures 4.43, 4.45, 4.47** and **4.49** for all catalysts used.

The k_{app} values were calculated using first order rate equation by plotting $\ln(C_t/C_o)$ vs time. The slope of the plot gives k_{app}. The plots are given in **Figures 4.44, 4.46, 4.48** and **4.50.** Tabulated k_{app} values for catalysts are given in **Table 4.4.**

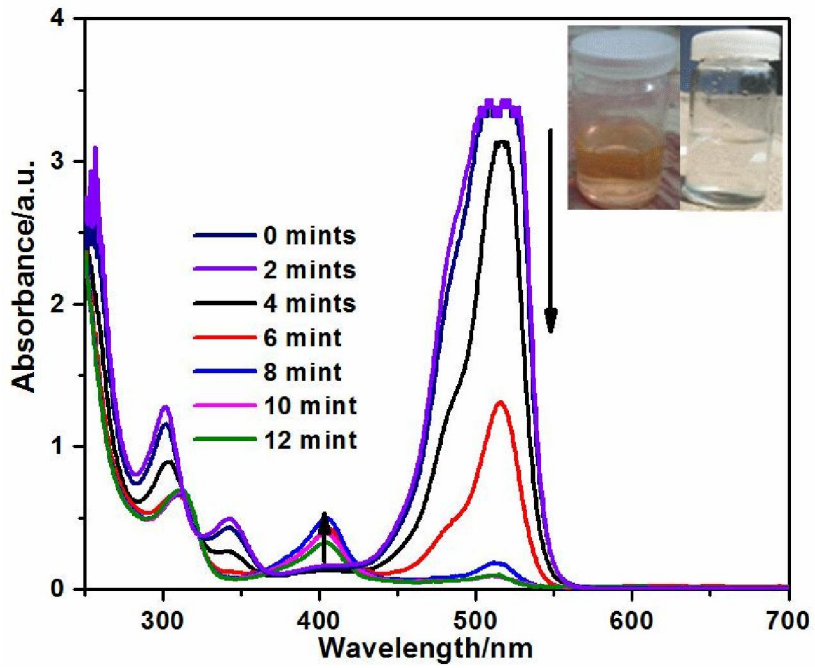

Figure.4.43. Degradation of EY through P01-Ag10

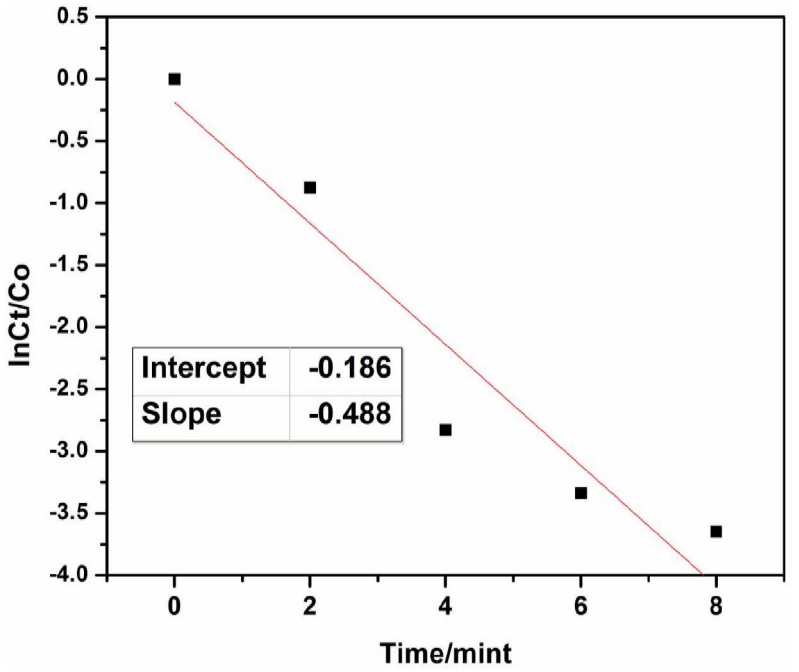

Figure.4.44. Plot of $\ln(C_t/C_o)$ vs. time for the degradation of EY by P01-Ag10

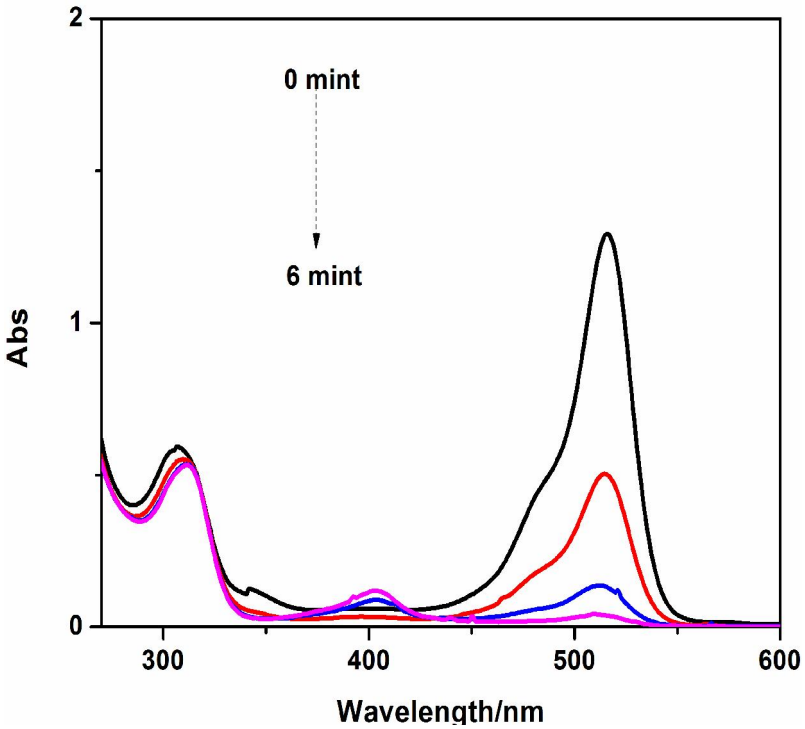

Figure.4.45. Degradation of EY through P01-Ag40

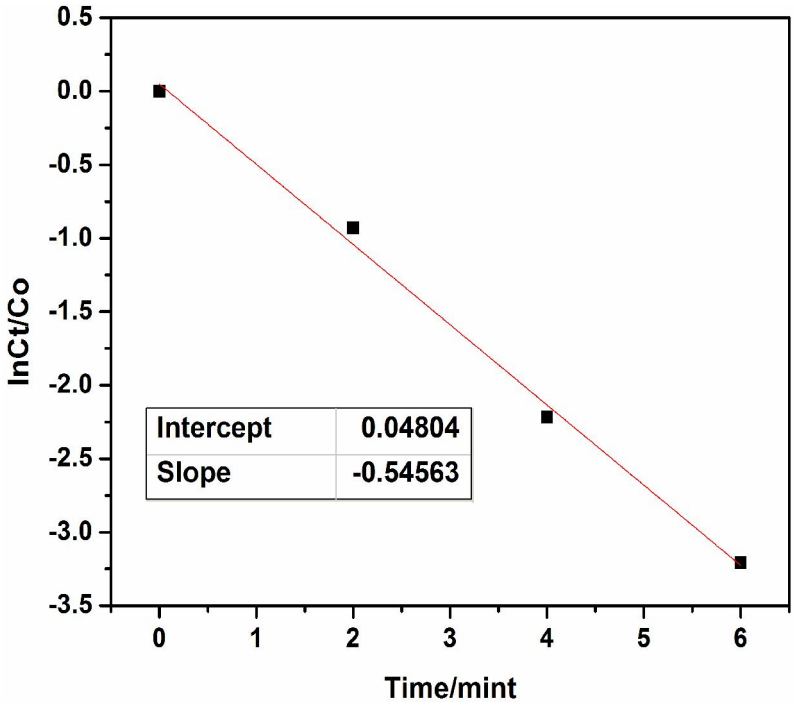

Figure.4.46. Plot of $\ln(C_t/C_o)$ vs. time for the degradation of EY by P01-Ag40

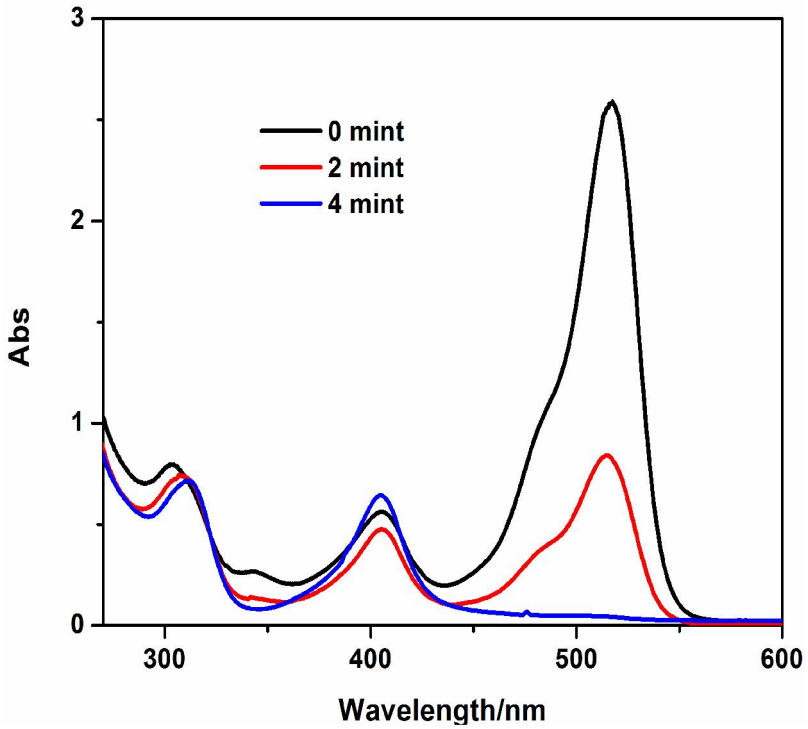

Figure.4.47. Degradation of EY through P01-Au10

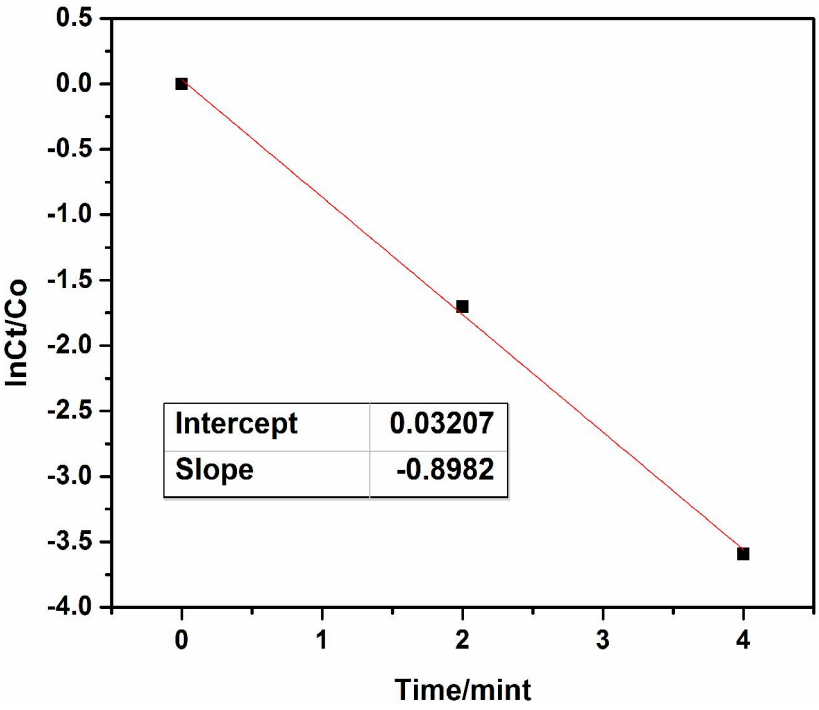

Figure.4.48. Plot of $\ln(C_t/C_o)$ vs. time for the degradation of EY by P01-Au10

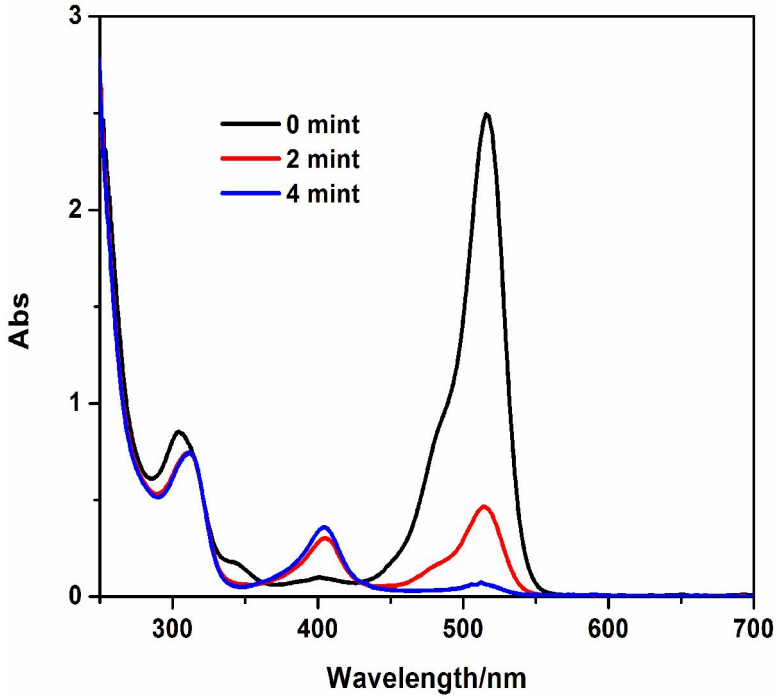

Figure.4.49. Degradation of EY through P01-Au40

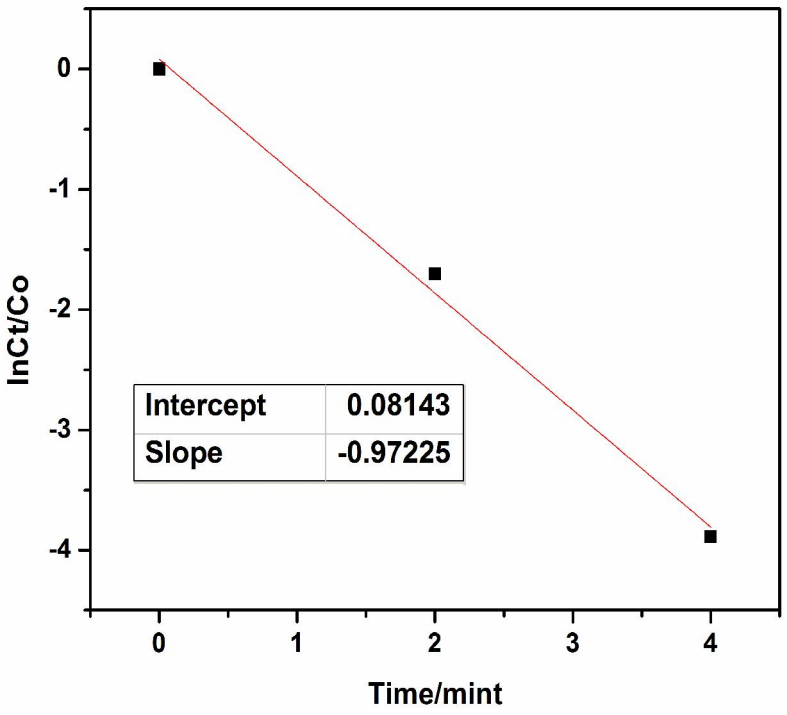

Figure.4.50. Plot of ln(Ct/Co) vs. time for the degradation of EY by P01-Au40

Table 4.4 k_{app} values obtained for the degradation of EY

Catalyst used	$k_{app} \times 10^2$ **S^{-1}**
P01-Ag10	0.81
P01-Ag40	1.0
P01-Au10	1.51
P01-Au40	1.62

4.8 Conclusion

The synthesis of pure and hybrid microgels were confirmed by FTIR spectroscopy. The pH and thermo responsive behavior of pure microgels were studied by DLS and the results showed that the hydrodynamic radius increases with increase in pH. Increase in temperature reduces the particle size at pH 2.6 while no effect was observed at pH 8.5. The effect of pH and temperature on SPR was also studied using UV-visible spectroscopy. The SEM images revealed the formation and homogeneous distribution of Ag and Au nanoparticles in polymer network. XRD results also confirmed the synthesis of pure and hybrid microgels. From the rate constant values it is clear that hybrid microgels synthesized at 40^{o}C act as a good catalyst as compared to others synthesized at 10 ^{o}C. It was found that Au based catalysts were more efficient than Ag based catalysts. Catalytic activity was enhanced with increasing temperature. All the catalysts were stable, recyclable and can be used as a catalyst for reduction of materials in organic reactions.

4.9 Future Work

Future work is mainly concerned to find the end products produced during the degradation of dyes and functionalization of the catalysts for the enhancement of their catalytic activity.

Chapter-5
References

1. S.A. Baeurle. "Multiscale modeling of polymer materials using field-theoretic methodologies: a survey about recent developments". *Journal of Mathematical Chemistry*, **2009**, 46 (2), 363–426.
2. Ferry, John D. (**1980**) Viscoelastic Properties of Polymers. New York: Wiley, ISBN ___0471048941
3. Li, Y.T., T. , *J. Chem. Phys,* **1989**. 90: p. 5161-5166.
4. Li, Y.T., T. , *J. Chem. Phys,* **1990**. 92: p. 1365-1371.
5. Oh JK, Drumright R, Siegwart DJ, Matyjaszewski K. The development of microgels/nanogels for drug delivery applications. *Prog Polym Sci* **2008**;33: 448-77.
6. Oh JK, Lee DI, Park JM. Biopolymer-based microgels/nanogels for drug delivery applications. *Prog Polym Sci* **2009**; 34:1261-82.
7. M.J. Murray, M.J.S., *Adv. Colloid Interface Sci*, **1995**. 54: p. 73.
8. .Karg M, Pastoriza-Santos I, Perez-Juste J, Hellweg T, Liz-Marzan LM. Small **2007;** 3:1222-9.
9. .Sorrell CD, Carter MCD, Serpe MJ. *Advanced Functional Materials* **2011**;21(3):425-33.
10. Debord JD, Lyon LA. *Journal of Physical Chemistry B* **2000**; 104(27):6327-31.
11. Hellweg T, Dewhurst CD, Bruckner E, Kratz K, Eimer W. *Colloid and Polymer Science* **2000**;278(10):972-8.
12. Schmidt S, Zeiser M, Hellweg T, Duschl C, Fery A, Moehwald H. *Advanced Functional Materials* **2010**;20(19):3235-43.
13. Jeong B, Gutowska A. Trends in Biotechnology **2002**; 20(7):305-11.
14. Gao, J. and B.J. Frisken, Influence of reaction conditions on the synthesis of self-cross-linked N-isopropylacrylamide microgels. *Langmuir*, **2003**. 19(13): p. 5217-5222.
15. Hoare, T.R.a.D.S.K., Hydrogels in drug delivery: progress and challenges. *Polymer,* **2008**. 49(8): p. **1993-2007**.
16. W. Funke, B., *Polym. J*, 1**989**. 21: p. 107.

17. Gao, J.a.B.J.F., Influence of reaction conditions on the synthesis of self-cross-linked N-isopropylacrylamide microgels. *Langmuir*, **2003**. 19(13): p. 5217 5222.
18. den Berg, A.a.G.á.V., Redox-responsive organometallic microgel particles prepared from poly (ferrocenylsilane) s generated using microfluidics. Chemical Communications, **2014.** 50(23): p. 3058-3060.
19. Hugo Almeida, M.H.A.a.P.L., *Journal of Applied Pharmaceutical Science,* **2012**. 02 (06): p. 01-10.
20. .R.H. Pelton, P.C., *Colloids Surf.,* **1986**. 20: p. 247–256.
21. C. Wu, S.Q.Z., *Macromolecules*, **1997**. 30: p. 574–576.
22. M.J. Garcia-Salinas, M.S.R.-C., F.J. de las Nieves, *, J. Colloid Interface Sci*, **2002**. 248: p. 54–61.
23. Pelton, R.H., *Advances in Colloid and Interface Science*, **2000**. 85: p. 1-33.
24. E. Daly, B.R.S., *Langmuir,* **2002**. 16: p. 5546–5552.
25. M.J. Murray, M.S., . () *Adv. Colloid Interface Sci*, ***1995***. 54: p. 73.
26. Khan, A., *Journal of Colloid and Interface Science,* **2007**. 313: p. 697–704.
27. Burdukova, E.L., H.; Bradshaw, D. J.; Franks, G. V., Miner. Eng, **2010.** 23: p. 921–927.
28. Sun, S.a.P.W., A . one-step strategy for thermal-and pH-responsive graphene oxide interpenetrating polymer hydrogel networks. *Journal of Materials Chemistry*, **2011.** 21(12): p. 4095-4097.
29. Schultz, S.S., R. D, Mock, J. J.; Schultz, A. D. Proc. Natl., Acad. Sci. U.S.A, **2000.** 97:996.
30. C. Shi, M. Cheng, Z. Qu, X. Bao, Investigation on the catalytic roles of silver species in the selective catalytic reduction of NOx with methane, *Appl. Catal*. B. 51 ***(2004)*** 171–181.
31. Y. Lu, Y. Mei, M. Ballauff, Thermosensitive core-shell particles as carrier systems for metallic nanoparticles*, J. Phys. Chem*. B 110 **(2006)** 3930–3937.
32. Y. Lu, Y. Mei, M. Drechsler, M. Ballauff, Thermosensitive core-shell particles as carriers for Ag nanoparticles: modulating the catalytic activity by a phase transition in networks, Angew. Chem. Int. Ed. 45 (**2006)** 813–816.
33. L. Xie, M. Chen, L.M. Wu, Fabrication and properties of hollow

poly(Nisopropylacrylamide)-Ag nanocomposite spheres*, J. Polym. Sci.* A: *Polym. Chem*. 47 (**2009)** 4919–4926.

34. Y. Dong, Y. Ma, T. Zhai, F. Shen, Y. Zeng, H. Fu, J. Yao, Silver nanoparticles stabilized by thermoresponsive microgel particles: synthesis and evidence of an electron donor–acceptor effect, Macromol. Rapid Commun. 28 (**2007)** 2339–2345.
35. Y.M.Mohan, T. Premkumar, K. Lee, K.E. Geckeler, Fabrication of silver nanoparticles in hydrogel networks, Macromol. Rapid Commun. 27 (**2006)** 1346–1354.
36. T. Coradin, C. Roux, J. Livage, J. *Mater. Chem*. 12 (**2002)** 1242.
37. A. Corma, M. Moliner, M.J. Diaz-Cabanas, P. Serna, B. Femenia, J. Primo, H. Garcia, *New J. Chem*. 32 (**2008)** 1338.
38. V. Puchol, J.E. Haskouri, J. Latorre, C. Guillem, A. Beltran, D. Beltran, P. *Amoros, Chem.* Commun. (**2009**) 2694.
39. K. Aslan, J.R. Lakowicz, C.D. Geddes, *Anal. Chem*. 77 (7) (**2005) 2007–2014**.
40. M. Shibayama, F. Ikkai, S. Inamoto, S. Nomura, C.C. Han, *J. Chem. Phys*. 105 **(1996)** 4358.
41. T. Mishra, R.K. Sahu, S.-H. Lim, L.G. Salamanca-Riba, S. Bhattacharjee, Hexadecylamine capped silver and gold nanoparticles: comparative study on formation and self-organization, *Mater. Chem. Phys*. 123 (**2010**) 540–545.
42. M. Chen, Y.-G. Feng, X. Wang, T.C. Li, J.-Y. Zhang, D.-J. Qian, Silver nanoparticles capped by oleylamine: formation, growth, and self-organization, Langmuir 23 (**2007**) 5296–5304.
43. Liu CF, Maruyama T, Yamamoto T. *Polym J* **1993**;25:363.
44. Luqman A. S.; Wulian, C.; Mohammad, S.; Jianhua, H.; Angang, D. and Dong.,Y. Thermal and pH Dual Responsive Copolymer and Silver Nanoparticle Composite for Catalytic Application, *Chinese Journal of Chemistry*, **2015** 33, 467-472
45. Kim, J.-H. and T.R. Lee, Hydrogel-templated growth of large gold nanoparticles: synthesis of thermally responsive hydrogel-nanoparticle composites*. Langmuir,* **2007**. 23(12): p. 6504-6509.

46. Eismann, M.T. and C.R. Schwartz. Focal plane array nonlinearity and nonuniformity impacts to target detection with thermal infrared imaging spectrometers. in AeroSense'97. **1997**. International Society for Optics and Photon.
47. Karge, H., et al., UV-Visible Spectroscopic Investigations and Related Studies on Coke Formation over Industrial H-ZSM-5-based Catalysts. *Studies in Surface Science and Catalysis,* **1989**. 49: p. 1327-1337.
48. Lv, L.-P., Stimuli-responsive materials for self-healing in corrosion protection, **2014,** Johannes Gutenberg-Universität Mainz.
49. Hassan, P.A., S. Rana, and G. Verma, Making sense of brownian motion: colloid characterization by dynamic light scattering. Langmuir, **2014**. **31**(1): p. 3-12.
50. Berne, B. and R. Pecora, Laser light scattering from liquids. Annual review of physical chemistry, **1974**. 25(1): p. 233-253.
51. Clark, N.A., J.H. Lunacek, and G.B. Benedek, A study of Brownian motion using light scattering. Am. J. Phys, **1970**. 38(5): p. 575-585.